12-2015

Simulation of Lateral Migration and Sedimentation of a Flexible Fiber in a Vertical Weak Shear Flow

Ali Ibrahim Neamah Neamah
Western Michigan University

SIMULATION OF LATERAL MIGRATION AND SEDIMENTATION OF A FLEXIBLE FIBER IN A VERTICAL WEAK SHEAR FLOW

by

Ali Ibrahim Neamah Neamah

A thesis submitted to the Graduate College
in partial fulfillment of the requirements
for the degree of Master of Science in Engineering
Chemical Engineering
Western Michigan University
December 2015

Thesis Committee:

Dewei Qi, Ph.D., Chair
Said Abubakr, Ph.D.
James Springstead, Ph.D.

SIMULATION OF LATERAL MIGRATION AND SEDIMENTATION OF A FLEXIBLE FIBER IN A VERTICAL WEAK SHEAR FLOW

Ali Ibrahim Neamah Neamah, M.S.E.

Western Michigan University, 2015

This research is a thorough numerical investigation and critical analysis of lateral migration of a deformable particle settling in a vertical weak shear flow. Under the vertical weak shear fluid, the deformable particle may move either to the coagulation area, or the dispersion area, depending on Reynolds numbers, shear Reynolds number, fiber flexibility, and aspect ratio. In this study, a lattice Boltzmann equation is used to solve Navier-Stokes equation and a flexible particle method is employed to attack the problem of motion of a flexible fiber. A bounce-back rule is used to deal with moving boundaries interacting with fluids. Several simulations are first conducted at the same shear Reynolds number, particle settling Reynolds number and aspect ratio except that the rigidity is varied at different levels. It is found that the rigidity plays a critical role, may change particle lateral migration direction, either migrate toward a coagulation area, or toward a dispersion area, depending the value of the rigidity. It shows that the rigidity may alter the fiber inertia, in turn, convert coagulation to dispersion. In other words, flexibility may alter the stability of fiber suspension. At a low settling Reynolds number, as the vertical shear flow increases the fiber dispersion trend increases and the lower rigid fiber has a larger tendency to disperse.

ACKNOWLEDGMENTS

I would like to offer my thanks to Dr. Qi for his support and advice during the process of this research. And I would like to thank Dr. Said and Dr. Springstead for their advice throughout the research. I would also like to thank Western Michigan University, Chemical Engineering program for presenting me with the opportunity to enhance my education. I would like to thank the Higher Committee for the Education Development in Iraq (HCEDiraq) for support and fund me throughout my study in the U.S. and from my deep down heart, I would like to thank my father, mother, brothers, sisters and all my friends for their encouragement to me throughout my study. And finally, I would like to thank Jessica Postma and the writing center at WMU for their review of this research.

Ali Ibrahim Neamah Neamah

TABLE OF CONTENTS

Table of Contents—Continued

LIST OF FIGURES

List of Figures—Continued

CHAPTER I

INTRODUCTION

Sedimentation is a very important separation method in industry, which is normally used to separate the solid particles from liquids. This method is utilized in various fields such as: oil refineries, potable water treatment, Industrial water treatment, and many other techniques. By using a lattice Boltzmann equation and a flexible particle method, migration and rotation of a flexible fiber in a vertical weak shear flow are simulated at different parameters, such as the shear Reynolds number, viscosity, fiber flexibility, and particle density, which may impact on particle settling and result in a variety of phenomena. It is critical to understand how and why these parameters affect particle coagulation and dispersion. To study effect of flexibility on lateral migration, the flexibility is systematically varied at different levels for a given shear Reynolds number and a given particle Reynolds number. It is demonstrated that the flexibility alters the fiber inertial effect, in turn, convert coagulation to dispersion at a selected Reynolds number. In the simulations, the shear Reynolds number (R_S) is set at 0.1, 0.2 and 0.3 and the settling particle Reynolds number ranges from 0.1 to 1.36. The fiber aspect ratio is fixed at 5. The results of the lateral migration and rotation at different flexibilities and Reynolds numbers are recorded and used to analyze the states of solid particle coagulation and dispersion.

1.1 Current Research

In this study, I focused on the flexible fiber setting in a vertical weak shear flow and analyzed the influence of the shear flow on a flexible fiber. Sedimentation is the process of particles settling by gravity in a fluid. When fibers are settling, a weak vertical shear flow may be established within the suspension. In other words, the weak vertical shear flow is generated from the variation of the fiber number density in the fluid. A fiber within the suspension may experience the shear force and laterally migrate either toward the downward flowing fluid region with the high particle number density, which is called coagulation area, unstable suspension region, or toward the lower particle number density region which is called dispersion area, stable suspension region, depending on the settling Reynolds numbers, defined by $R_{sd} = V_f . l / 2\upsilon$, where V_f is the terminal settling velocity of the mass center of the fiber in the gravity direction or y-direction; l is the half fiber length; and ν is the kinematic viscosity [3].

In the present work, it has been used a flexible solid particle. The flexible particle settles at different levels of shear Reynolds numbers, sediment Reynolds number, particle density and flexibility. It has been studied how the variation of these parameters affect the particle motion. Lattice Boltzmann method is a sufficient method to simulate the interaction between a fluid and solid particles when the March number is less than 0.3 or when the ratio of the size of the solid particle to the whole width of the flow channel is small.

Two operations, collision and streaming, have been included mathematically in the algorithm of Lattice Boltzmann method and the algorithm is simple for fluid domain. In addition, the Lattice Boltzmann code for Navier-Stokes equations could be implemented

in a few hundred lines in Fortran or any other programming language. This simplicity essentially comes from two major reasons. First, when one derives the Navier Stokes equation from the LB equation, the fluid distribution function is expanded to the second order of the small Knudsen numbers (the ratio of the mean free length to the characteristic spatial scale of the whole fluid system), called Chapman-Enskog expansion or multi-scale analysis, and so that collision, convection, and diffusion time scales are separated. This greatly simplifies the algorithm. Second, the fluid collision matrix of the LB equation is linearized by Bhatnagar-Groos-Krook (BGK) approximation. Therefore, the efficiency of lattice Boltzmann method is much higher than that of the traditional finite element and differential equations. This research allows ones to better understand the role of flexibility on lateral migration and fiber rotation, the effect of shear Reynolds number and sediment Reynolds number, and the effect of the fiber density on the direction of the lateral migration of the particle (Qi and et al, 2013) [3].

This research is vital since it benefits various disciplines - from chemical engineering to physics and geography. This research also interprets and discusses the fluctuations and rotation of the fiber through the migration within the fluids by analyzing the overall behavior and direction of the motion of solid particles.

In this research, the behavior of flexible fibers settling through a weak vertical shear flow is specifically analyzed. This analysis is conducted via a simulation program. Numerous tests are conducted to determine the effect of the factors on the flexible fiber migration. A variety of shear Reynolds numbers in each test is utilized. All the phenomena are explained based on results. All the points are discussed later in this thesis.

1.2 Literature Review

An extensive research has been conducted sedimentation of a single rigid fiber at different shear rates in fluids and different aspect ratios by Dewei Qi et al. The research is entitled "Lattice Boltzmann Simulations of Sedimentation of a Single Fiber in a Weak Vertical Shear Flow" [3]. They have used Lattice Boltzmann method in order to simulate the interaction between the solid particles and a fluid, which is same the method that is used in this research. In addition, they have found that there are three phases of the lateral migration depending on settling Reynolds number R_{sd} and particle aspect ratio κ .

In phase 1, "At a low settling Reynolds number R_{sd} , the suspension becomes more stable $N_y < 0.5$. In turn, fibers migrate to the dispersion area. Moreover, the relative velocity in the left side is larger than the relative velocity in the right side. In addition, all fibers stop migrating when the wall repulsion force is equal to the lift force" [3].

In phase 2, as R_{sd} increases and excesses a critical settling Reynolds number R_{sd1} , the fiber suspension becomes unstable $N_y > 0.5$, and the fibers migrate to the coagulation area with an angle along the horizontal direction. At a low R_{sd} =1.028, fiber rotates and oscillates with angle θ =180 in y-direction, and fiber does not have a fixed orientation. At R_{sd} = 1.203, the fiber oscillates and then becomes stable [3]. At R_{sd} =1.74, 2.35, and 3.51, fibers have no oscillation. "As R_{sd} increases, fiber's lateral migration decreases because of the angle of the fiber approaches 90 degrees. As R_{sd}

exceeds $R_{sd\,2}$, the fiber inertial alignment might dominate R_s and keep migrating towards the coagulation area, and the fiber may stay in the center" [3].

In phase 3, at a sufficient large R_{sd}, the inertia dominates the weak shear flow and it may have little influence on stability. "When R_{sd} increases from 24.04 to 44.51, the amplitude of oscillation of both migration and orientation angle increases, the fiber position does not change very much. And migration is independent of sediment Reynolds number. The oscillation is influenced by the weak effect or vortex behind the fiber" [3]. And migration is impacted by the aspect ratio which is varied at κ =1.2, 1.6, and 2. At R_S =0.1, κ decreases, the final critical settling increases. "As aspect ratio decreases, the second sediment critical Reynolds number decreases because the fiber with smaller aspect ratio is easier to migrate with vertical velocity less than zero" (Dewie Qi and et al, 2013) [3].

CHAPTER II

THE RESEARCH OBJECTIVES

In this research, the main idea is that finding a better understanding to know how the roles of flexibility, shear Reynolds number, settling Reynolds number, fiber density influences lateral migration of a flexible fiber.

2.1 Previous Research

Extensive research has been conducted on rigid fibers. Qi et al studied the effect of shear flow on rigid fibers by changing the density of the fibers, the sediment Reynold number and aspect ratio with keeping the rigidity fixed. In current research, the effect of shear flow rates on flexible fibers has been studied. Understanding the shear flow rates effect on the flexible fibers is more difficult than that on the rigid fibers due to the flexible fibers are deformable more than rigid fibers. Note the aspect ratio in Qi et al.'s research is not fixed, while in this research is fixed.

2.2 Role of Flexibility on Lateral Migration and Rotation

To best understand the role of flexibility on lateral migration and rotation, a simulation code is utilized to see the impact on fiber migration. A flexible fiber can move in significantly more (potentially unknown) directions than a rigid fiber. Due to this factor, an analysis of the flexible fiber has more innate challenges -- especially when a fluid has a shear flow. This is a major aspect and one of the goals of this research to see

how a vertical weak shear flow impacts the direction and the migration of the fibers. Moreover, it has been found how the migration of the flexible fibers depends on other variables such as density, the shear flow, and the Reynold number, among others.

For example, if there are five fibers in one channel, the addition of a sixth fiber within the same channel becomes affected by the other five fibers' shear flow. In addition, this affects the movement (i.e. migration) of the sixth fiber. This is especially so for the flexible fiber because this kind of fiber is affected by the flexibility and this situation, the flexibility is dominated by the shear flow of the other fibers. Moreover, since the density of the other five fibers and their motion generates shear flow (so there is a shear flow for each fiber and the shear flows are overlapping with each other) and the shear flows impacts the sixth flexible fiber.

2.3 The Effect of a Shear Reynolds Number on Migration

The shear flow is generated by the movement of the number of fibers which has a density within the fluid. These shear flows are tangled with each other and this impacts the fiber through rotating the fiber and pushing it in a direction. The shear flow is influenced by the movement of the neighboring fibers in the fluid. In the simulation, the velocity is equal to zero at the left wall of the simulation box at Z=0 in the dispersion area. And the velocity is an unknown value at Z=L at the right side of the simulation box in the coagulation area, where Z is the horizontal direction. All of these variables affect the flexible fiber migration and these factors orient flexible fibers to different directions which are shown with details in the results chapter. This study also focus on these factors, and the relationship between the shear Reynolds number (R_s) and the migration of the

fibers. As Qi et al states (p. 8, 2013) the shear Reynold number has an important effect on the migration of the rigid fibers.

2.4 The Effect of a Sediment Reynolds Number on the Fiber

Next it has been analyzed the effect of sediment Reynolds number on the sedimentation. In addition, it has been studied how the flexible fiber behaves in the fluid when a fiber settles with using different flexibilities. Moreover, it has been analyzed the flexible fiber during the settling process and how it might experience a shear flow as well as how the fiber might go to the region with high fiber's densities (because this region has a lot of fibers and at this region there is a big shear flow since the large amount of particles within the fluid, and this region is called the coagulation area) or the fiber might go to the region which has a lower fiber density (this region is called the dispersion area). Either way, the settling motion depends on the settling Reynolds Number $R_{sd} = V_f .l / 2\nu$. V_f is defined as the terminal settling velocity of the mass center in the z-direction , and (l) defined as the half fiber length, and ν defined as the kinematic viscosity.

The Shear Reynolds Number plays an important role in the sedimentation process by using different Shear Reynolds Numbers for the settling of any flexible fiber. It might be known that the real effect of sediment Reynolds Number on the flexible fibers and how this effect controls the migration of the flexible fiber. In chemical plants, this especially can be utilized and applied in many cases. For instance, in water treatment, they put chemical materials into the water tanks to treat the industrial water; the process is continuous. Thus, water comes from the previous unit (at a certain velocity) and when

the water drops down in the tank through the input pipe, it has a shear flow. In this case, chemical materials are needed to treat the water, so it is important to know how these chemical materials have impacted the water. Therefore, after studying the effect of the sediment Reynolds number, the density of the fiber, the rigidity of the fiber, and the effect of the shear flow on the flexible fibers, it can be understood which direction the fiber goes and then we can analyze the reasons why the fibers went to this direction (and then it can be understand how to control the Shear Reynolds Number to force the fiber to go in a particular direction). The relationship between the density of the fiber and the settling Reynolds number is directly proportional. As density increases, the sediment Reynolds number increases.

Also the density of the fiber plays an important role in the sediment Reynolds number where if the fiber density increases, the sediment Reynolds number increases. And if the density of a fiber decreases, the sediment Reynolds number decreases too. So the density of a fiber is directly proportional with the sediment Reynolds number. It is one of my goals to see how a fiber's density changes a fiber migration. Therefore, multiple cases have been conducted for different uses of a fiber density which varied at ρ =1.1, 1.01, 1.001. It was seen that how the influences on the orientation of a fiber are impacted in regards to the existence of the shear flow. That is shown in the results chapter.

CHAPTER III

THEORY AND METHODOLOGY

The lattice Boltzmann method is a powerful tool to simulate interactions between solid particles and fluids, and it is the primary method utilized in this research. The lattice Boltzmann method's kinetic nature allows it to simulate "the complex geometry of things such as a flexible web" [2]. The Bhatanaga-Gross-Krook (BGK) single relation time model is used. In the lattice Boltzmann method, "fluid particles reside on the lattice nodes and move to the nearest neighbors along the links with unit spacing in each unit time step" [2]. The equations of Lattice Boltzmann BGK equation according to Qi [2] is:

Equation 1: $$f_\sigma(\vec{x}+\vec{e}_\sigma\delta t, t+\delta t) = f_\sigma(\vec{x},t) - \frac{1}{\tau}\left(f_\sigma(\vec{x},t) - f_\sigma^{eq}(\vec{x},t)\right)$$

$f_\sigma(\vec{x},t)$ is defined as the distribution of the fluid particle with a velocity of e_σ at position of $\vec{x}$ and time of t. $f_\sigma^{eq}(\vec{x},t)$ is the equilibrium distribution function. σ_t is the time interval and τ is the single relaxation time, and $f_\sigma^{eq}(\vec{x},t)$ is defined as:

Equation 2: $$f_\sigma^{eq}(\vec{x},t) = \omega_\sigma \rho_f \left[1 + 3(\vec{e}_\sigma.\vec{u}) + (\vec{e}_\sigma.\vec{u})^2 - \frac{3}{2}(\vec{u}.\vec{u})\right]$$

σ = 1, this represents the particles movement to the nearest neighbors. σ = 2, this represents the particles movement to the next nearest neighbors. σ = 0, this represents the particles rest at the nodes. The weight coefficient ω_σ depends on the discrete velocity set and dimensions of space. The right side of equation 1 represents a collision process and the assignment of the value of the right side to the left side represents a streaming process. "The models is a three- dimensional lattice Boltzmann model on a cubic grid

with rest particles present, and each node has six nearest neighboring nodes in diagonal directions as shown in figure 1. The fluid particles with population $f_\sigma(\vec{x},t)$ move along the 15 directions with velocity $\vec{e}_\sigma$. This discrete velocity set with 15 directions including the rest particles (accounted as one direction) is Equation 3 ", (Shuling.H, Ch.3, P.79. 2013).

Equation 3: $$\vec{e}_\sigma = \begin{cases} (0,0,0) \\ (\pm1,0,0) \quad (0,\pm1,0) \quad (0,0,\pm1), \sigma = 0, \sigma = 1, \sigma = 2 \\ (\pm1,\pm1,\pm1) \end{cases}$$

And the coefficient of weight is:

Equation 4: $$\omega_\sigma = \begin{cases} \frac{2}{9}, \sigma = 0 \\ \frac{1}{9}, \sigma = 1 \\ \frac{1}{72}, \sigma = 2 \end{cases}$$

Imposing Taylor expansion in the power series of δt and ignoring high order terms, equation 1 becomes [2]:

Equation 5: $$D_\sigma f_\sigma + \frac{\delta t}{2} D_\sigma^2 f_\sigma = -\frac{1}{\tau \delta t}(f_\sigma - f_\sigma^{eq})$$

Where:

$$D_\sigma = \partial_t + \vec{e}_\sigma . \nabla \vec{x}$$

$$\partial t = \frac{\partial}{\partial t} \; and \; \nabla \vec{x} = \frac{\partial}{\partial x}\vec{i} + \frac{\partial}{\partial t}\vec{j} + \frac{\partial}{\partial t}\vec{k}$$

When the fluid velocity is much smaller than the sound speed - or the March number is less than 0.3, equation 3 can be expanded in the power series of a small

Knudsen number ε. For the purpose, a short time scale $t_0 = \varepsilon t$, a long time scale $t_1 = \varepsilon^2 t$, and a space scale $\vec{x}_0 = \varepsilon \vec{x}$ is introduced so that operators $\partial_t = \varepsilon \partial_{t_0} + \varepsilon^2 \partial_{t_1}$ and $\nabla \vec{x} = \varepsilon \nabla \vec{x}_0$. The distribution function can also be expanded in the power series of ε as:

Equation 6: $$f_\sigma = f_\sigma^{(0)} + \varepsilon f_\sigma^{(1)} + \varepsilon^2 f_\sigma^{(2)}$$

Where the higher order terms is larger than ε^2 are ignored

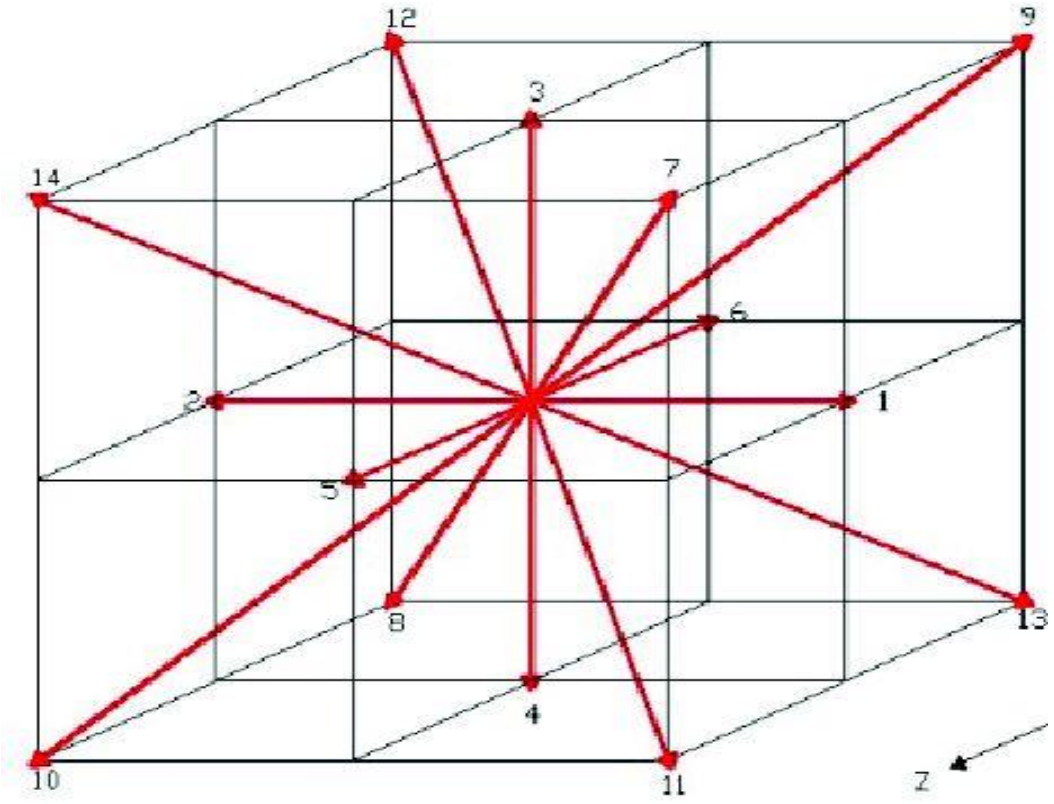

Figure 1: Schematic Diagram of a Cell of Space Discrete and Velocity Discrete $\vec{e}\sigma$ [2]

Equation 7: $$\varepsilon^0 : f_\sigma^{(0)} = f_\sigma^{eq}$$

Equation 8: $\varepsilon^1 \quad : \quad D_{0\sigma} f_\sigma^{(0)} = -\frac{1}{\tau \delta t} f_\sigma^{(0)}$

Equation 9: $\varepsilon^2 : \quad \partial_{t_1} f_\delta^{(0)} + (1 - \frac{1}{2\tau}) D_{0\sigma} f_\sigma^{(1)} = \frac{1}{\tau \delta t} f_\sigma^{(2)}$

Where, $D_{0\sigma} = \partial_{t0} + \vec{e}_\sigma . \nabla \vec{x}_0$ Calculating the zeroth and first orders of the moments of velocity $\vec{e}_\sigma$ of equations 7, 8, and 9, using $\sum_\sigma f_\sigma^{(k)} = 0$ and $\sum_\sigma \vec{e}_\sigma f_\sigma^{(k)} = 0$ for k > 0 and combining all equations on time scales t_0 and t_1, one can obtain the Navier-Stokes equation after some mathematical manipulation.

Equation 10: $\frac{\partial}{\partial t}(\rho \vec{u}) + \nabla(\rho u u) = -\nabla p + \nabla . \sigma$

Where $\vec{u}$ is the fluid velocity; p is the pressure, ρ_f the fluid density and $\rho_f \vec{u}$ momentum density. The fluid density and the momentum density are given by:

Equation 11: $\rho_f = \sum_\sigma f_\sigma \quad , \quad \rho f \vec{u} = \sum_\sigma f_\sigma \vec{e}_\sigma$

The kinematic viscosity ν is related to the relaxation time τ and is given by:

Equation 12: $\nu = 1/3\ (\tau - 1/2)$

The time interval δ_t becomes 1. In order to match the fluid velocity with the solid boundary velocity at the fluid-solid interface, a moving boundary condition is adopted.

Equation 13: $f_{\sigma'}(\vec{x}, t+1) = f_\sigma(\vec{x}, t_+) - 6\omega_\sigma \rho_f \vec{e}_\sigma . \vec{U}_b$

where t+ denotes the time after fluid particle collision, σ′ represents the reflecting direction and σ denotes the incident direction of fluid particle at a node adjacent to the solid-surface of a solid rigid particle (having a finite volume) with the boundary velocity $\vec{U}_b = \vec{U}_c + \vec{\Omega} \times \vec{x}_b$; $\vec{U}_c$ is the velocity of the mass center of the solid particle, $\vec{\Omega}$ is its

angular velocity; $\vec{x}_b = \vec{x} + \frac{1}{2}\vec{e}_\sigma - \vec{R}_i$; $\vec{x}$ is the position of the node; $\vec{R}_i$ is the mass center of solid particle. The hydrodynamic force exerted on the solid particle at the boundary node is computed by:

Equation 14: $\vec{F}(\vec{x} + \frac{1}{2}\vec{e}_\sigma) = 2\vec{e}_\sigma(f_\sigma(\vec{x}, t_+) - 3\omega_\sigma \rho_f \vec{U}_b.\vec{e}_\sigma)$

The total hydrodynamic force on the solid particle is produced by:

Equation 15: $\vec{F}_i^h = \sum \vec{F}(\vec{x} + \frac{1}{2}\vec{e}_\sigma) \pm \rho_f(\vec{x}, t)\vec{u}(\vec{x}, t)$

The summation is over all the boundary nodes on the fluid region associated with the solid particle. The second term on the right hand side of the equation 15 considers the local fluid momentum contribution whenever a fluid node either enters or leaves the solid region. The positive sign is used when the fluid node enters the solid region and the minus sign is used when the solid node becomes the fluid node so that the momentum is conserved. In addition, an equilibrium distribution function with the fluid velocity equal to the solid boundary velocity is added on the newly formed fluid nodes. The total torques on the solid particle is used when the solid node becomes the fluid node so that the momentum is conserved. In addition, an equilibrium distribution function with the fluid velocity equal to the solid boundary velocity is added on the newly formed fluid nodes. The total torques equation on the solid particle is shown below: (Qi et al, p.12, 2013) [2].

Equation 16: $\vec{T}_i^h = \sum (\vec{x} + \frac{1}{2}\vec{e}_\sigma - \vec{R}) \times \left((\vec{F}(\vec{x} + \frac{1}{2}\vec{e}_\sigma) \pm \rho_f(\vec{x}, t)\vec{u}(\vec{x}, t)\right)$

For the flexible particle method, during motion of the flexible particle, the following condition has to be satisfied at any time:

Equation 17: $\vec{R}_{i+1} - \vec{C}_{i+1}^+ = \vec{R}_i + \vec{C}_i^+ \quad , \quad i = 1, N-1$

Where N is the total number of segments; $\vec{R}_i$ is the mass center of the segment; and $\vec{C}_i^+$ is the vector from its mass center to the joint i, where i runs from 1 to N − 1 and the segments are labelled by index i in an increasing order [1].

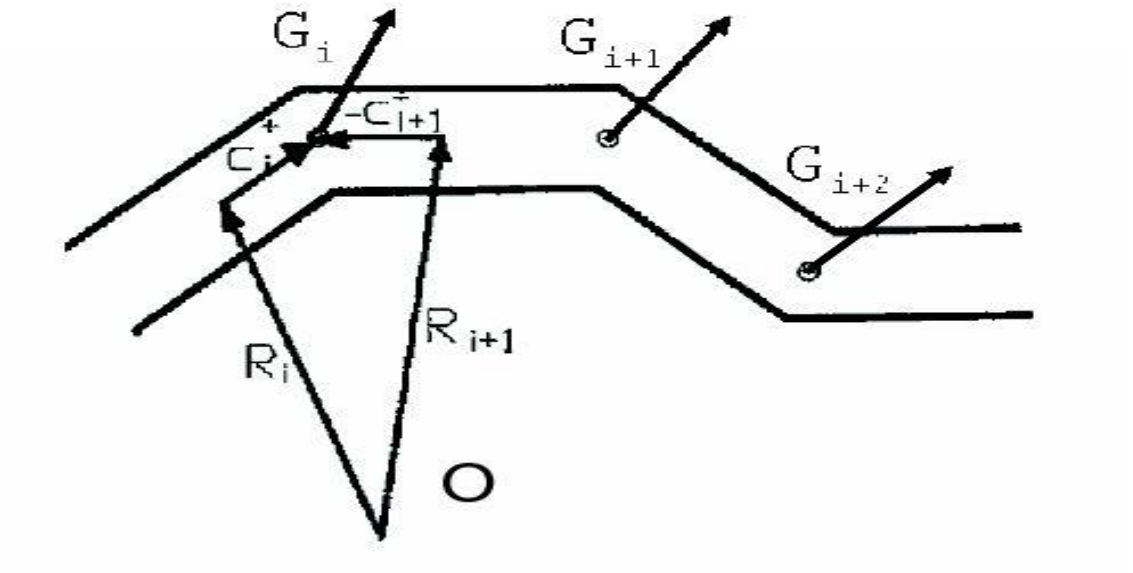

Figure 2: The Segments are Connected Through Joints [2]

Gi is the constraint force vector on the ith segment; Ri is the position vector of the mass center of the ith segment; C+i is the vector of the semi-axis of the main body of the ith segment [2].

In fact, $\vec{C}_i^+ = A_i^{-1}\vec{c}_i^+$ where constant vector $\vec{c}_i^+ = a_3(0,0,1)$ is the semi-axis of the segment and fixed along the Z′-direction or the chord direction in a body-fixed coordinate system; a3 = c / (2N); A_i is the rotational transformation matrix of segment i from the

space coordinate system to the body-fixed coordinate system. The prime sign denotes the body fixed coordinate system. Equation 17 can be rewritten as:

Equation 18: $\vec{R}_{i+1} - \vec{A}_{i+1}\,\vec{c}^{+}_{i+1} = \vec{R}_i + A_i^{-1}\,\vec{c}^{+}_i \quad i = 1, N-1$

The segments are linked by rotational springs and can be rotated. The bending moments are proportional to their deformational angles as:

Equation 19: $\vec{T}_i^{b} = EI_l \dfrac{\Theta}{2a_3}\hat{b}_i$

Where $\hat{b}_i = \dfrac{\hat{z}_i \times \hat{z}_{i+1}}{\left|\hat{z}_i^{'} \times \hat{z}_{i+1}^{'}\right|}$ is the unit normal to the bending plane where $\hat{z}_i^{'}$ is the unit vector in the chord direction of the ith segment in the body-fixed coordinate. For the present case, $\hat{b}_i$ is a constant equal to $\hat{X}_i.\Theta_i$ is the bending angle between the ith and (i+1) th segments in the chord direction [2].

CHAPTER IV

SIMULATION SETUP

Various computational simulation cases have been conducted. These simulation cases display and describe the overall effects (within the established parameters) of the directions of the fiber within a fluid. A code program has been used to describe the interaction between the flexible fibers settle in a fluid. The weak shear flow that is being used in a vertical direction in the simulation box, and it is changing along Z-direction as it is clear in figure 3. The initial velocity is zero at the left wall of the simulation box at Z=0, in the dispersion area, and the velocity in the right wall is calculated based on shear Reynolds number (R_s), and viscosity (ν) at Z=L, in the coagulation area. V is unknown.

Parameters must be established and considered according to the size and dimensions (X, Y, and Z) of the box used for the simulation. The dimensions of the fiber (diameter and length) must also be specified. In addition, the rigidity of the fiber must be considered. Rigidity is not fixed, so it is most likely changed in the numerous runs of the simulation. The viscosity of the fluid is fixed at υ =0.16, and the fiber density is varied at (ρ =1.1, 1.01, 1.001). And shear Reynolds number is varied at (R_S = 0.1, 0.2, 0.3). Furthermore, the sediment Reynolds number ranges from 0.1 to 1.36 and that based on the density and velocity of the flexible fiber. The fiber aspect ratio (κ) is fixed at 5. The fiber consists from nine segments, each segment has a length (4.444), so the total length of the fiber is roughly 40. It should be taken in consideration that the confinement ratio, which is the ratio between the width of the simulation box (Z=80) and the length of the

fiber (L=40), and here the confinement ratio is 2. Furthermore, each segment of the flexible fiber has an angle during the migration and that makes the flexible fiber deformable during the migration, and that is explained with figures in the results chapter.

The Reynolds Number (R_s), is calculated by using the simulation program where it is the velocity gradient or shear flow times the half of the length of the fiber (l), all of which is multiplied by the half of the length of the fiber. This will all then be divided by the viscosity.

Equation 20: $$R_S = \frac{G\frac{l}{2}.\frac{l}{2}}{v}$$

G is the shear flow or velocity gradient. This is calculated by the division of the velocity of the fluid U_z over the width of the simulation box Z. And shear flow is calculated by:

Equation 21: $$G = U_Z/L \ , (\ L = Z + 1)$$

The sediment Reynolds Number is calculated by multiplying the velocity of the fiber (V_f) times the half of the fiber length all divided per the fluid viscosity:

Equation 22: $$R_{sd} = \frac{V_f.l}{2v}$$

The program has been run in the simulation box, with size (X=40, Y= 214, Z = 80). This box is rectangle in shape, therefore the volume can be found by multiplying X, Y, and Z. And all the variables and parameters are dimensionless.

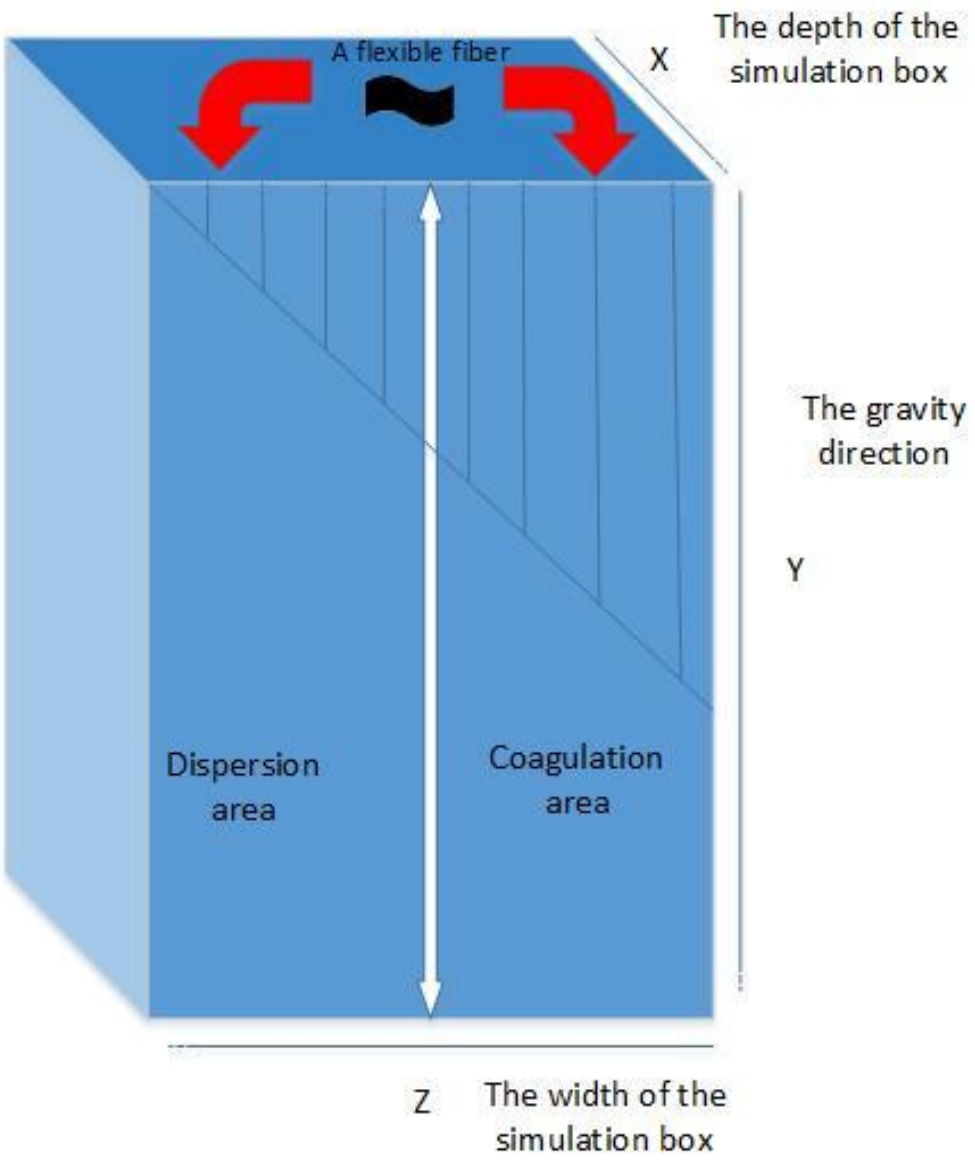

Figure 3: The Simulation Box

All flexible fibers are located at the center of Z-direction, at Z=0.5, between the two walls as it is shown in figure 3. All flexible fibers are going to migrate along Y-direction due to the gravity after a short time of the settling, the flexible fibers rotate along Z-direction due to the shear flow. In addition, the fiber's rotation is limited on two

directions (Z, Y), which is called ZY-plane. In turn, the rotational polar angle Θ between the fiber and the vertical direction or Y-direction can be defined.

With regard to the fiber, the diameter is (D=8), and the length is (L=40). The aspect ratio is defined as the ratio between the length of the fiber per the diameter of the fiber, it is dimensionless. Aspect Ratio = L/D= 40/8=5. Note the aspect ratio is 5 and it is fixed for all simulation cases. The density is used in the simulation as a ratio between the density of the solid (particle) to the density of the liquid (fluid), so it is dimensionless.

Particular emphasis in this research is placed on the analysis of the flexibility of the fiber with using different Reynolds shear flows and different densities. Water has been used as a fluid in the simulation box. As we know the viscosity of water is constant, so in the experiments, we assume adding a material will change water's viscosity by using silica material which is going to increase the water's viscosity in the simulation.

The rigidity of the fiber is a vital variable, if the rigidity of the fiber is high, then the flexibility of the same fiber is low. Therefore, the rigidity and the flexibility have proportional direction.

This research conducts various runs of numerous cases with different values of rigidity (E.I), and Reynolds shear flow (R_s). This has three different values in the simulation (R_s = 0.1, R_s =0.2, and R_s =0.3). R_{sd} is varied in the simulation, there is R_{sd} for each fiber. In each case of the simulation, the program is run to recognize the rigidity and R_s effects on the fiber migration. All variable's units are dimensionless and the time interval which has been used in the simulation is the ratio between t over $t_\circ$. Moreover, (t) represents the regular time and ($t_\circ$) represents the ratio between the velocity of the

shear flow (U) per the length of the shear flow L, which is the width of the simulation box (Z). Therefore, the result of dividing t per t_0 is dimensionless. The repulsion force is set up at the two walls. At Z=0, Z=L there are repulsion forces. The benefit of these repulsion forces is stopping the fiber during the migration, when the fiber gets close to the wall in the dispersion or coagulation area. Otherwise the fiber will cross the simulation box's boundaries.

CHAPTER V

RESULTS

Cases with simulation box sizing (X=40, Y=214 and Z=80) are performed and analyzed in this research. In this sizing, Y is the vertical direction for settling down fibers which are driven by both gravity and shear flow. Z is the horizontal direction. , A lot of parameters such as density, shear Reynolds number and fiber rigidity may influence the pattern of settle down and they are varied in five cases of the simulation. We analyzed 5 groups of simulation cases. Each group has four fibers. Each fiber has a different rigidity and a different sediment Reynolds number. Most of the cases have different shear Reynolds numbers range (0.1-0.3). All variables are dimensionless.

5.1 Large Settling Reynolds Number Cases ($0.1= R_s < R_{sd} >1.0$)

To study effects of rigidity on lateral migration, the simulations are conducted in the same conditions expect that the rigidity is varied at four different levels (EI=62.76, EI=104.61, EI=209.22, and EI=470.74). In these simulations, the fiber density and shear Reynolds number are kept in the same level of 1.1 and R_s = 0.1, respectively. The results of settling Reynolds number fall in the range of 1.35 - 1.33 which is larger than 1. Therefore, fiber inertia plays an important role in these cases. In this Reynolds number range, the fiber attempts to align its long axis with the horizontal direction due to the inertial torque. This torque may be balanced by the imposed weak vertical shear force (R_s =0.1), resulting in an inclined angle between the fiber axis and the horizontal plane. The inclined

angle of the fiber axis with the horizontal direction drives fiber to migrate with a speed of $V_Z > 0$. On the other hand, the wall repulsive force has an opposite direction and force the fiber to be stopped before reaching the wall as shown in figure 4. Most fibers are oscillating, migrating to the region of $Z>0.5\,N_Z$, and stopped, on average of Z, at somewhere between the channel center $Z= 0.5\,N_Z$ and the wall $Z= N_Z$, where the inhomogeneity is reinforced. In other words, when R_{sd} >1, all fibers migrate to the higher fiber number density area and instability of the fiber suspension is enhanced.

However, the instability is affected by fiber rigidity. As rigidity varies, the final average lateral position of fiber is varied. The fiber with the least rigidity has a final position mostly close to the channel center, indicating that the most flexible fiber of EI=62.76 has a position of least values of $Z=0.63\,N_Z$, suggesting that The least rigidity has least tendency to migrate to the coagulation area. As the rigidity increases, the final position is more close to the wall of $Z= N_Z$. The fiber with the rigidity EI=209.22 is stopped at the position with the largest $Z=0.666\,N_Z$. As the rigidity continues to increase to a level of EI=470.74, the position becomes less close to the wall again. It is observed that intermediate rigidity has a position mostly close to the wall, illustrating the intermediate rigidity has a largest tendency to be coagulated. It is obvious that the rigidity has a profound influence on the instability of a suspension.

Most likely, the optimized flexibility of a fiber may have a larger inertial migration momentum, resulting in a larger inertial effect, which may be favorable to the formation of the inclined angle and drive the fiber migrate to the wall of $Z= N_Z$.

The small inclined angles of about 15 degree with the horizontal direction are shown in figures 7 and 8 and confirmed in the angular distribution function of figure 5. Figure 6 shows the fibers' velocities in the gravity direction. Figure 7 shows the angle of the ninth segment of a fiber, and the most rigid fibers do not have wide angles. Unlike, the most flexible fibers are the most deformable fibers, and that makes the fibers have wide angles during the migration. Figure 8 shows the angle average of all fiber's segments.

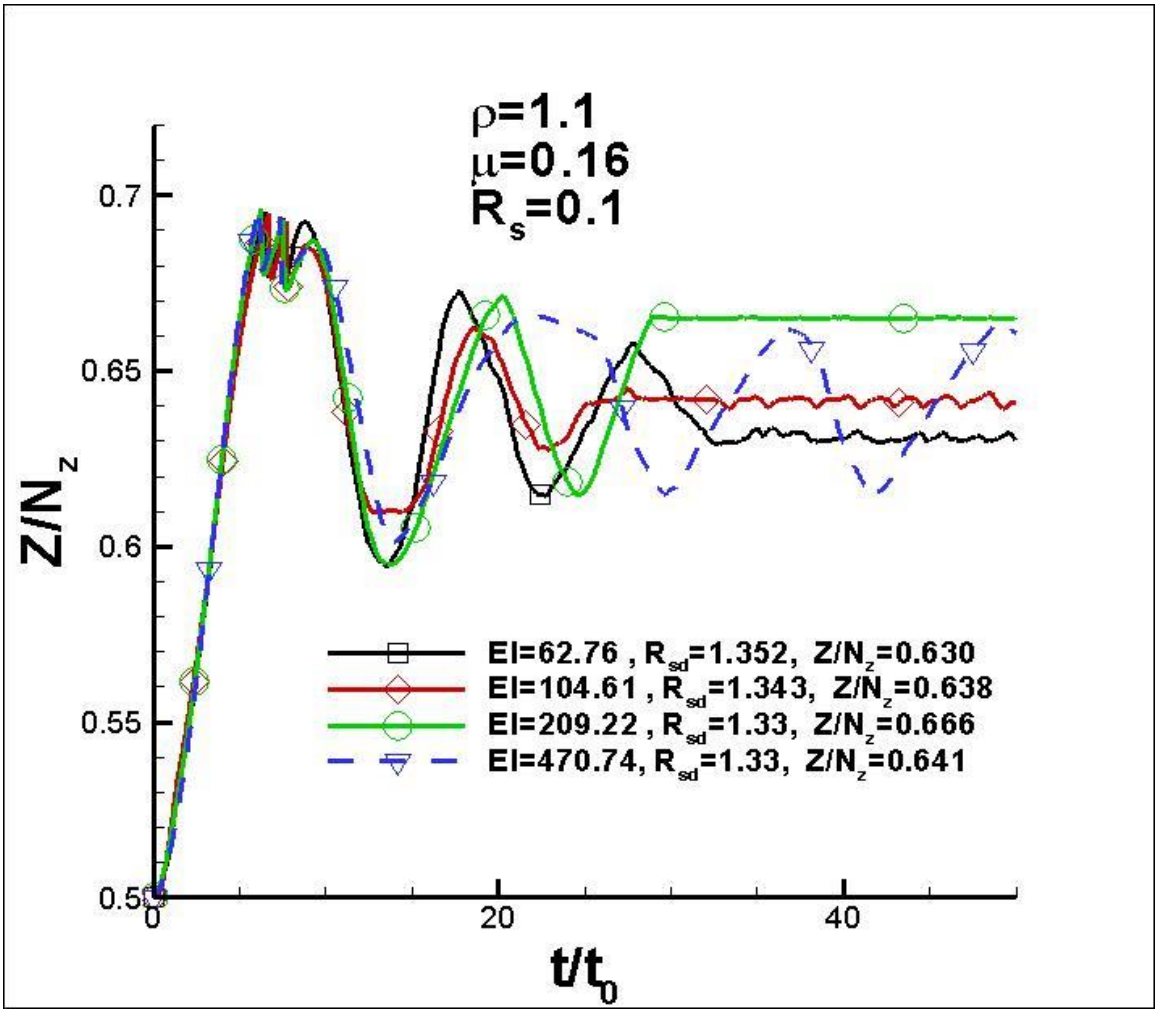

Figure 4: The Fiber Lateral Migration in a Vertical Shear Flow

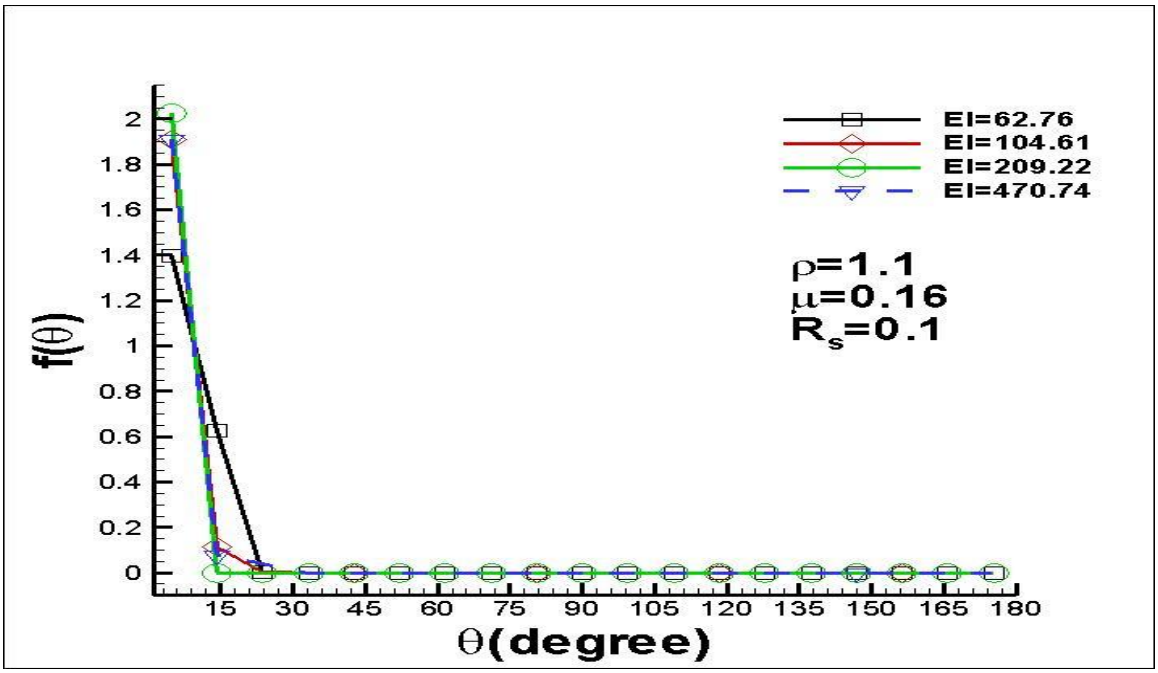

Figure 5: The Angle Probability of the Fiber During the Migration

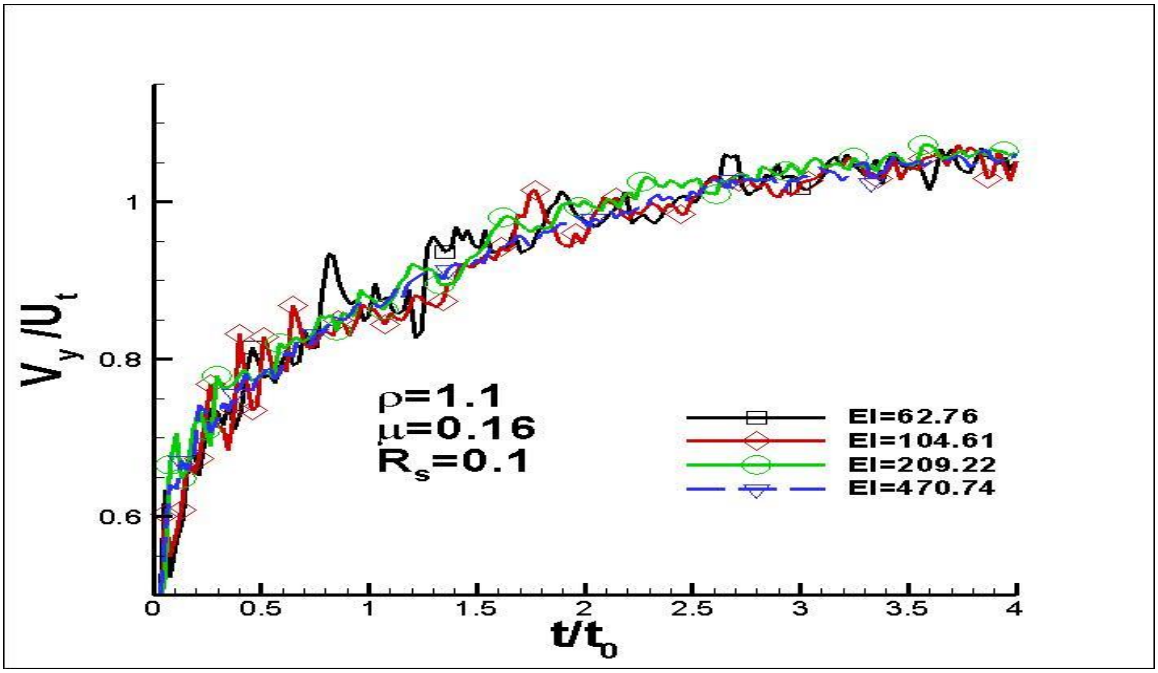

Figure 6: The Fiber's Velocities in the Gravity Direction of a Weak Vertical Shear Flow

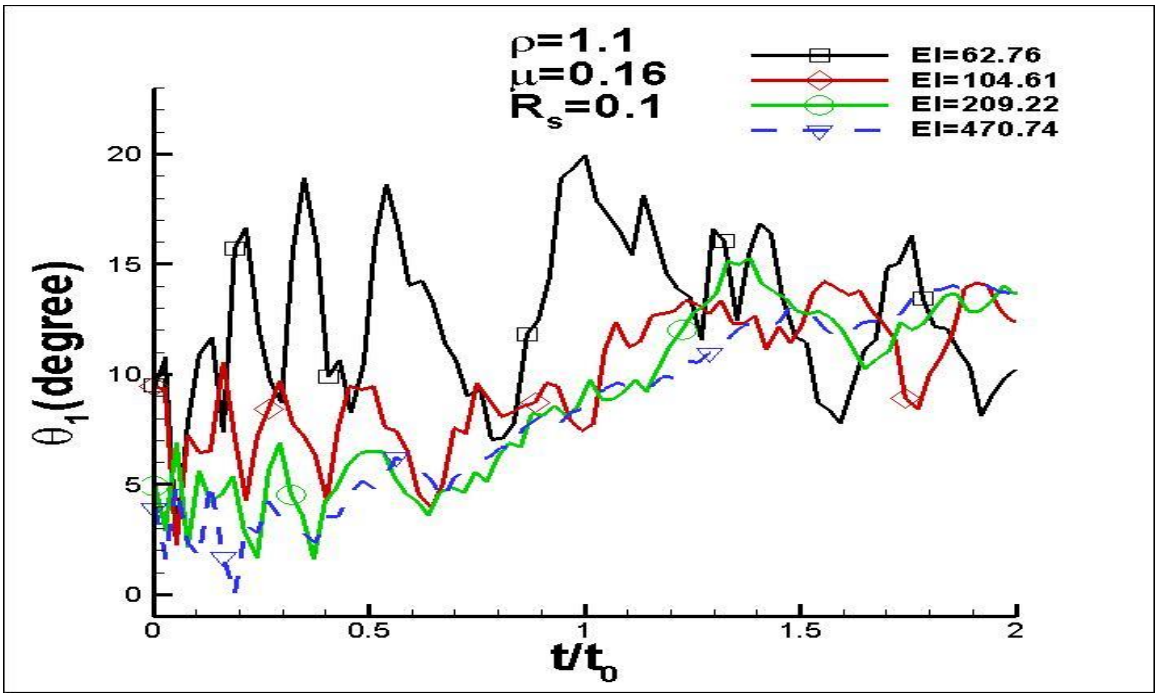

Figure 7: The Angle of the Ninth Segment of the Fiber in a Weak Vertical Shear Flow

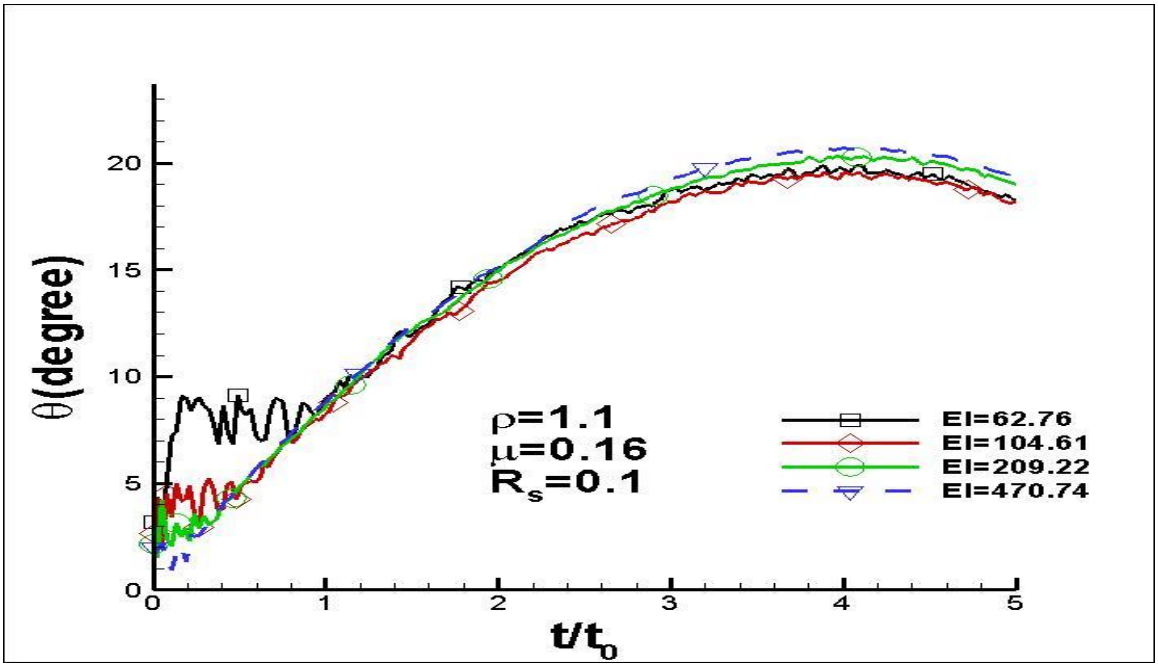

Figure 8: The Angle Average of the Fiber in a Weak Vertical Shear Flow

5.2 The Settling Reynolds Number Smaller than 1 ($R_S < R_{sd} < 1$)

To investigate effect of settling Reynolds number on motion, Simulations are carried out at a lower density of 1.01 while keeping R_S=0.1. The rigidity is varied at different levels of EI=31.38, EI=62.76, EI=209.22, and EI=470.74. All fibers settle down in a viscous fluid (υ =0.16) with a weak vertical shear flow. All cases have a lower Reynolds number less than 1 around 0.59-0.65.

It is observed that the fiber with the smallest rigidity EI=31.38 oscillates first and finally is stopped at a position of Z=0.48 N_Z, which is smaller than 0.5 N_Z as shown in figure 9, demonstrating that the most flexible fiber tends to migrate to the lower fiber density area and fiber distribution becomes more homogenous. This suspension is more stable. As the rigidity increases, the fiber oscillates. The average final position for all other rigidity is larger than Z=0.5 N_Z and these fibers migrate toward the coagulation area.

Figure 9 shows the position of each fiber during the migration. Figure 11 shows the angle probability of each fiber. Figure 12 shows the fibers' velocities in the gravity direction. Figure 13 shows the angle of the ninth segment of a fiber, and the most rigid fibers do not have wide angles. Unlike, the most flexible fibers are the most deformable fibers, and that makes the fibers have wide angles during the migration. Figure 14 shows the angle average of all fiber's segments.

The most flexible fiber with EI=31.38 migrates and rotates due to the shear flow (see figure 9, 11). The influence of the shear flow is larger than that of the fiber's inertial effects.

It is revealed that the flexibility can convert a fiber suspension from an unstable state to be a stable state.

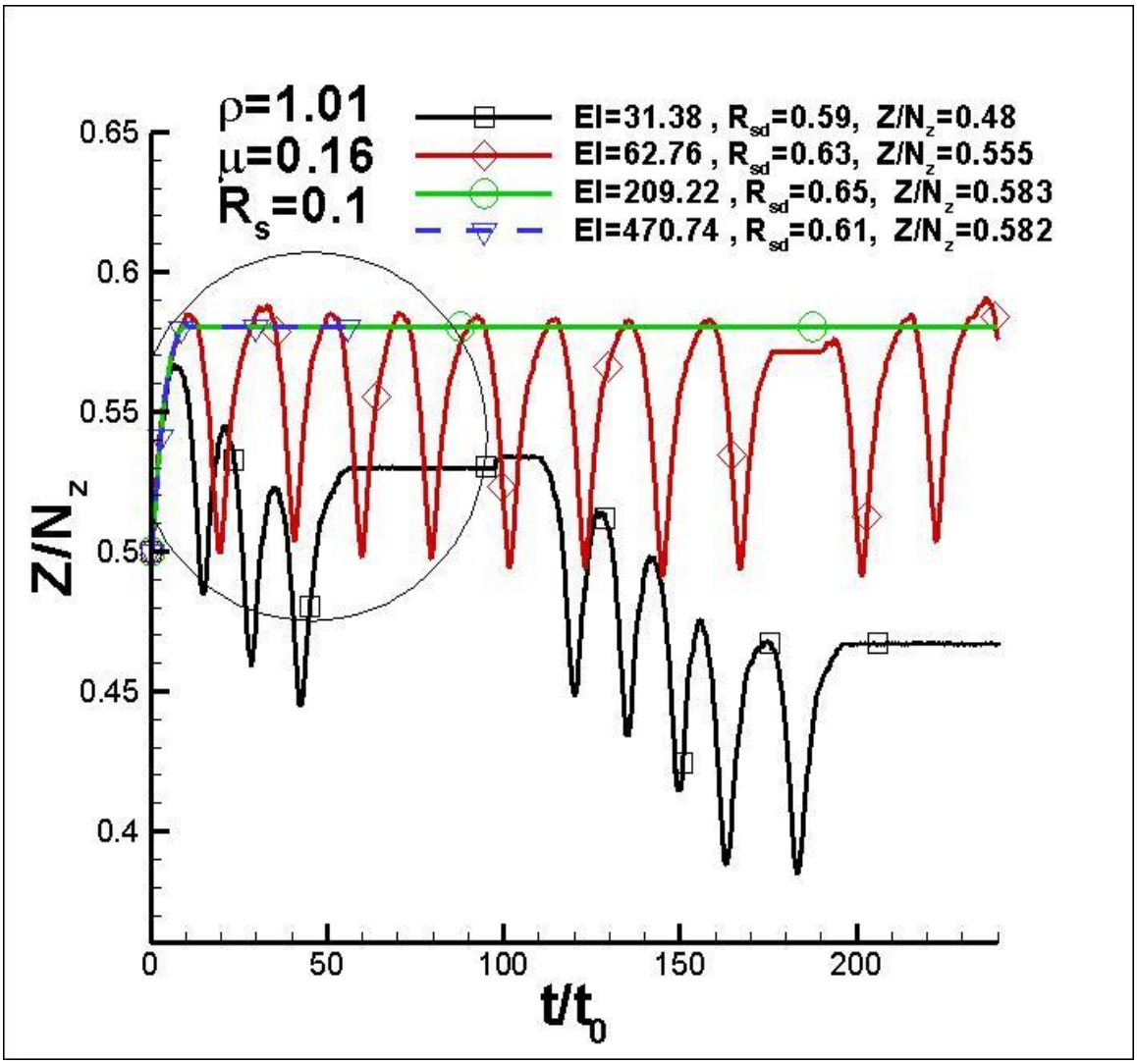

Figure 9: The Fiber Lateral Migration in a Vertical Shear Flow

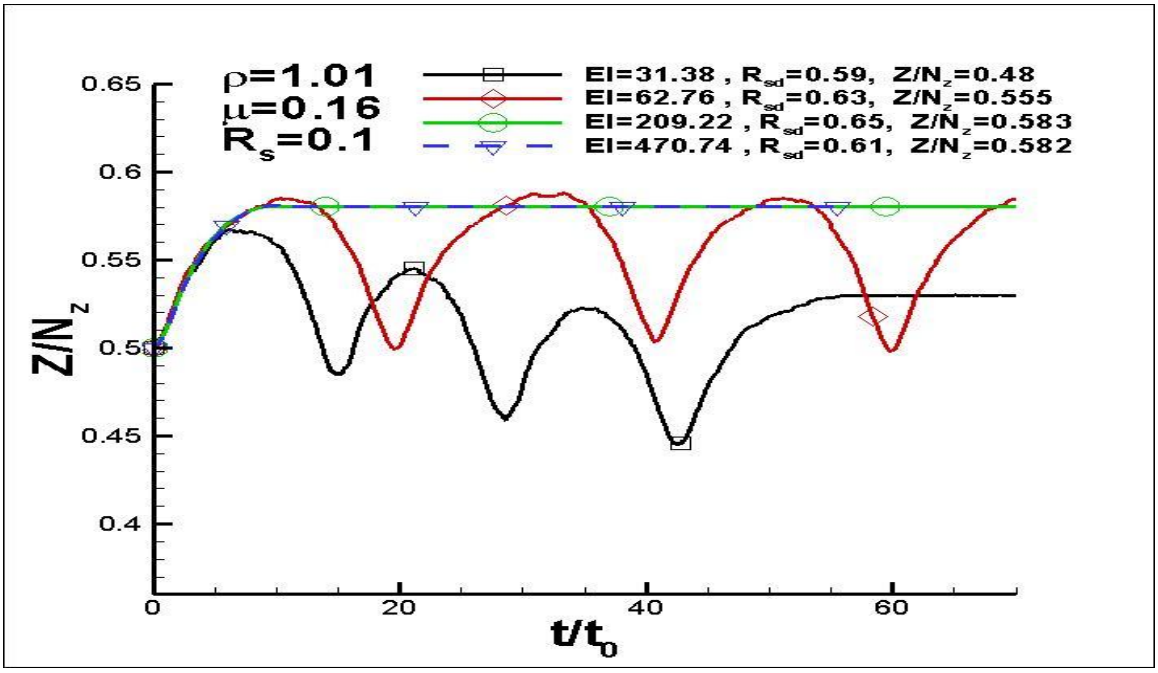

Figure 10: Magnification of Figure 9

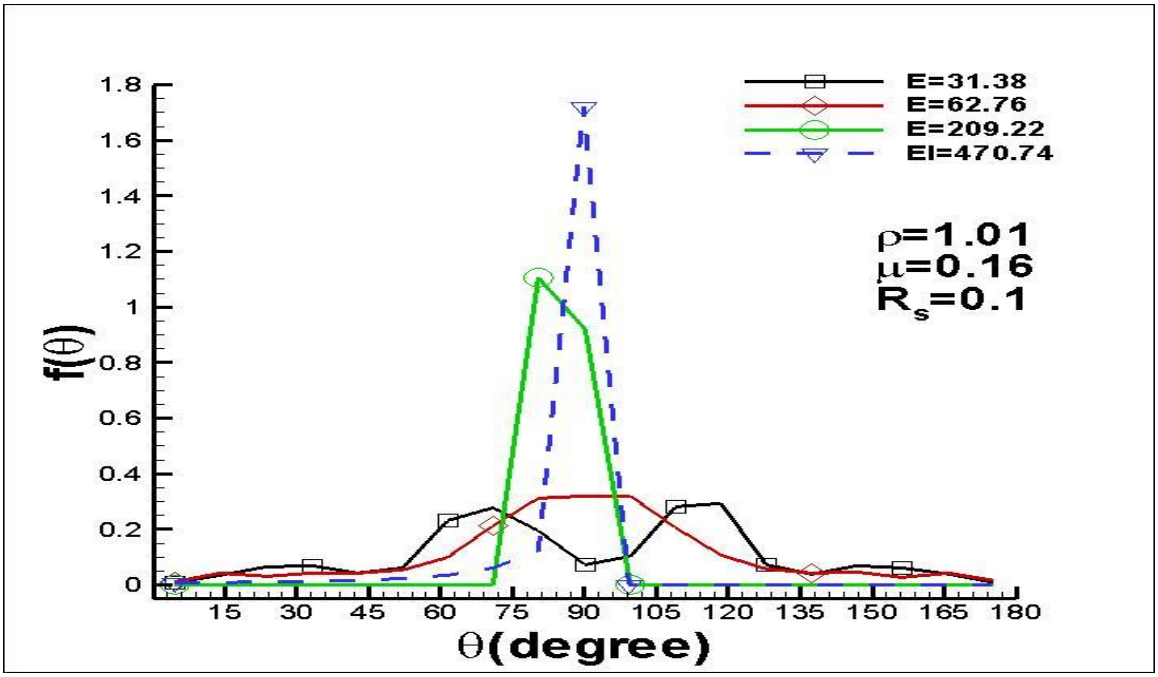

Figure 11: The Angle Probability of the Fiber During the Migration

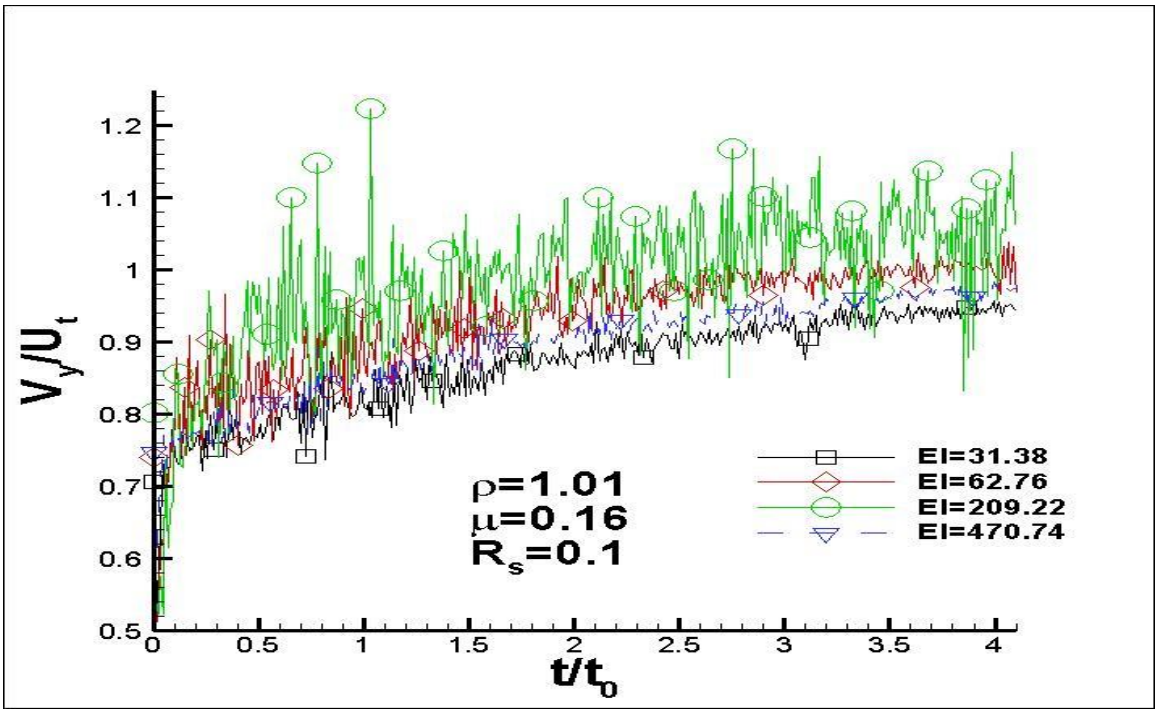

Figure 12: The Fiber's Velocities in the Gravity Direction of a Weak Vertical Shear Flow

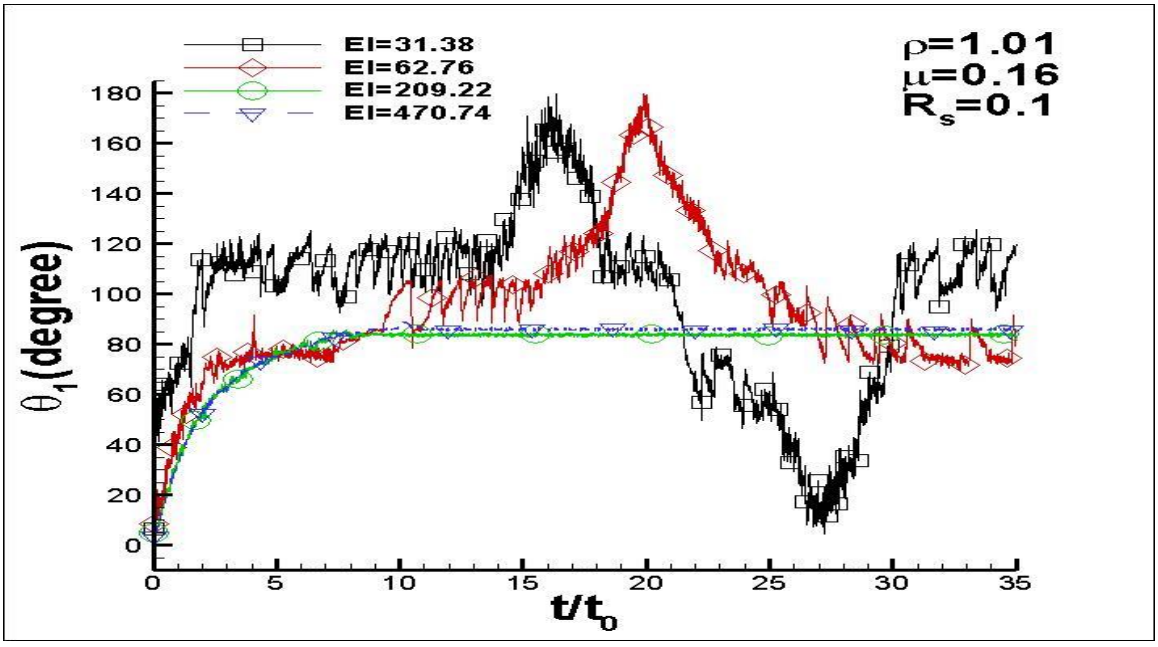

Figure 13: The Angle of the Ninth Segment of the Fiber in a Weak Vertical Shear Flow

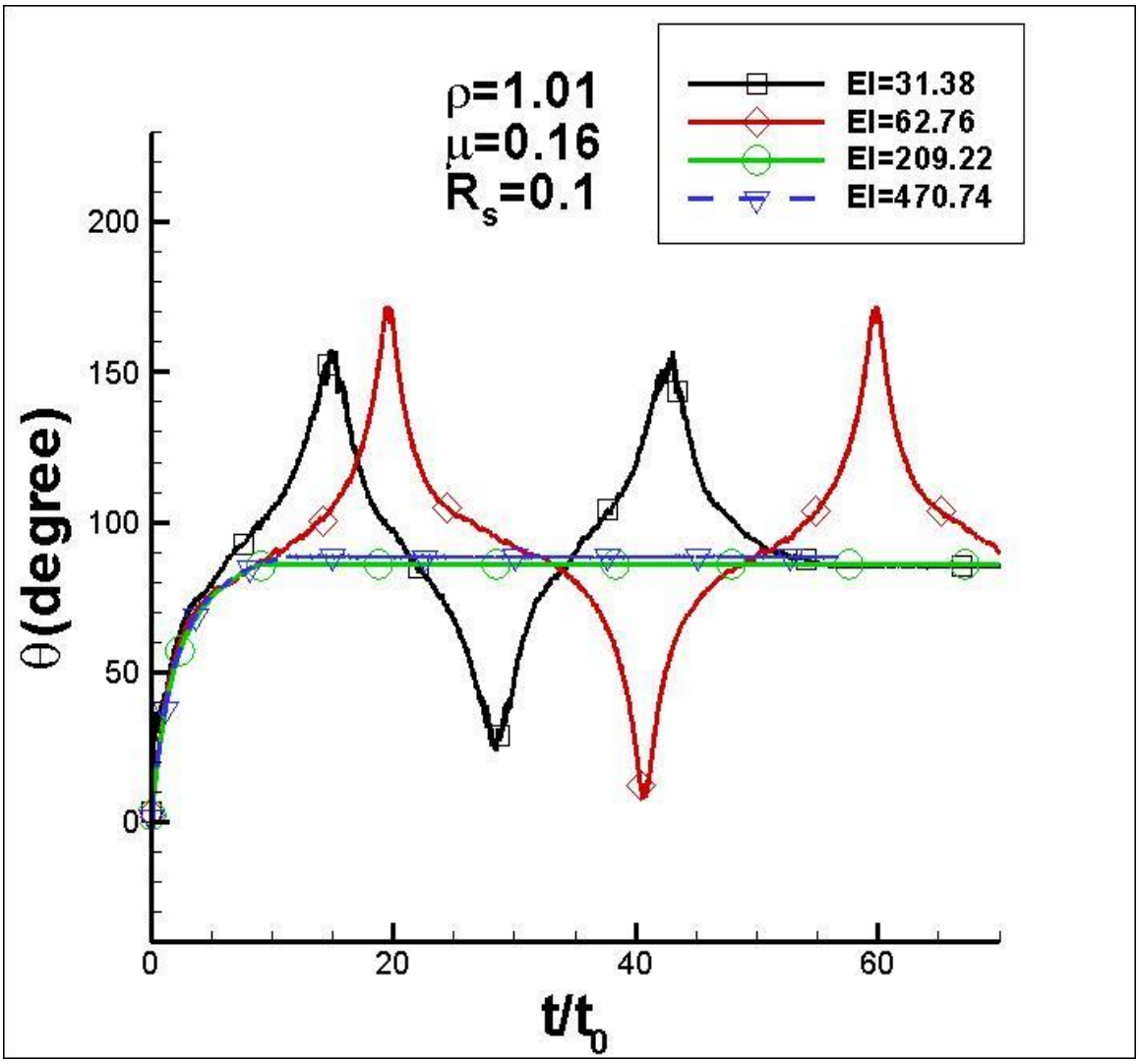

Figure 14: The Angle Average of the Fiber in a Weak Vertical Shear Flow

5.3 The Smallest Sediment Reynolds Number Cases

Attention has been turned to smaller Reynolds number cases. When the density (ρ) is 1.001, the shear Reynolds number (R_S) is 0.1, four different levels of rigidity (EI=31.38, EI=62.76, EI=209.22, and EI=470.74) are used again. The results of fiber lateral positions are shown in figures 15 and 16. When the rigidity of EI=31.38 is the smallest, the fiber oscillates and migrates to a position of $Z=0.33\,N_Z$, which is far smaller than the case of the previous dispersion case with $Z=0.48\,N_Z$. The fiber has a larger tendency to disperse, as compared with the previous case. For the most flexible case, the fiber migrates and rotates as shown in figure 20 for the angle average. The settling Reynolds numbers for all cases are very small around 0.21-0.24. This means that the fiber inertia is comparable with shear force. For the most flexible case of EI=31.38, the shear flow drives the fiber to rotate and migrate to the dispersion area. In this case, the fiber inertia can be ignored and the shear flow dominates fiber inertia. However, as the rigidity increases, the fiber becomes more stiff and inertia increases, the fiber alignment due to inertia is balanced by the shear force, resulting in stable angle around 80 degree. Therefore, the final positions are slightly larger than $Z=0.5\,N_Z$ for all other cases. In other words, they migrate to the coagulation area and becomes unstable.

Figure 15 shows the position of each fiber during the migration. Figure 17 shows the angle probability of each fiber. Figure 18 shows the fibers' velocities in the gravity direction. Figure 19 shows the angle of the ninth segment of a fiber, and the most rigid fibers do not have wide angles. The most flexible fibers are the most deformable fibers,

and the fiber has a wide angle distribution during the migration. Figure 20 shows the angle average of the fiber

The intermediate rigid fiber with EI=62.76 is the most coagulated fiber due to the flexibility of the fiber is influenced by the shear Reynolds number which makes the fiber deformed and takes a position between the vertical and horizontal directions. In turn, this direction makes the fiber little bit farther than others towards the wall in the coagulation area. The fibers with (EI=62.76, EI=209.22, and EI=470.74) coagulate close to each other with taking the consideration that the difference in the sediment Reynolds number.

Based on density, we compare this case with the cases in the last section. The previous case has a density of 1.1, while this case has a density of 1.001. It is seen that the fibers with a large density migrate toward the coagulation area farther than the fiber in this case. It is clear that as the fiber's density or settling Reynolds number increases, the tendency of the fibers migration toward the coagulation area increases.

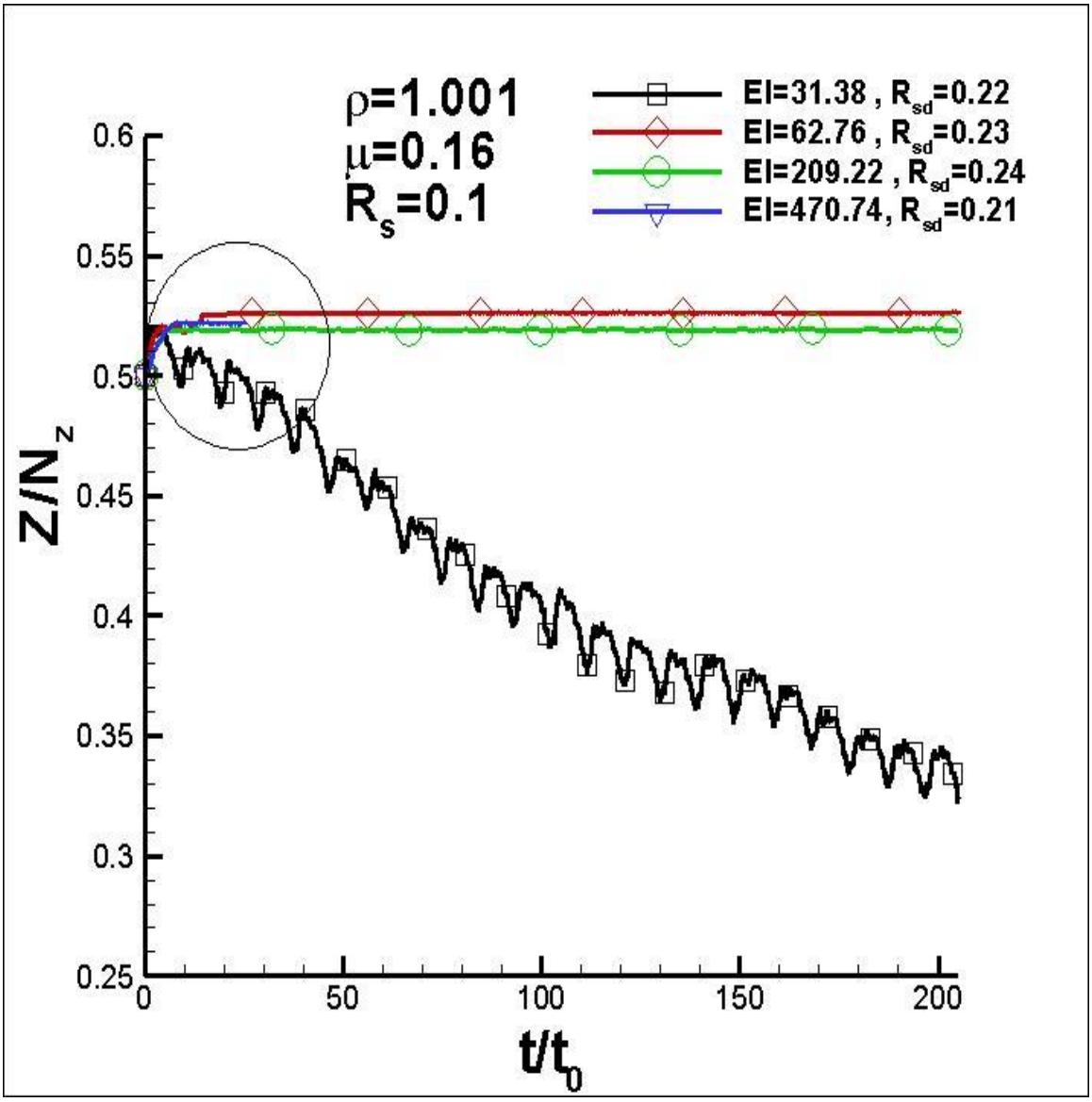

Figure 15: The Fiber Lateral Migration in a Vertical Shear Flow

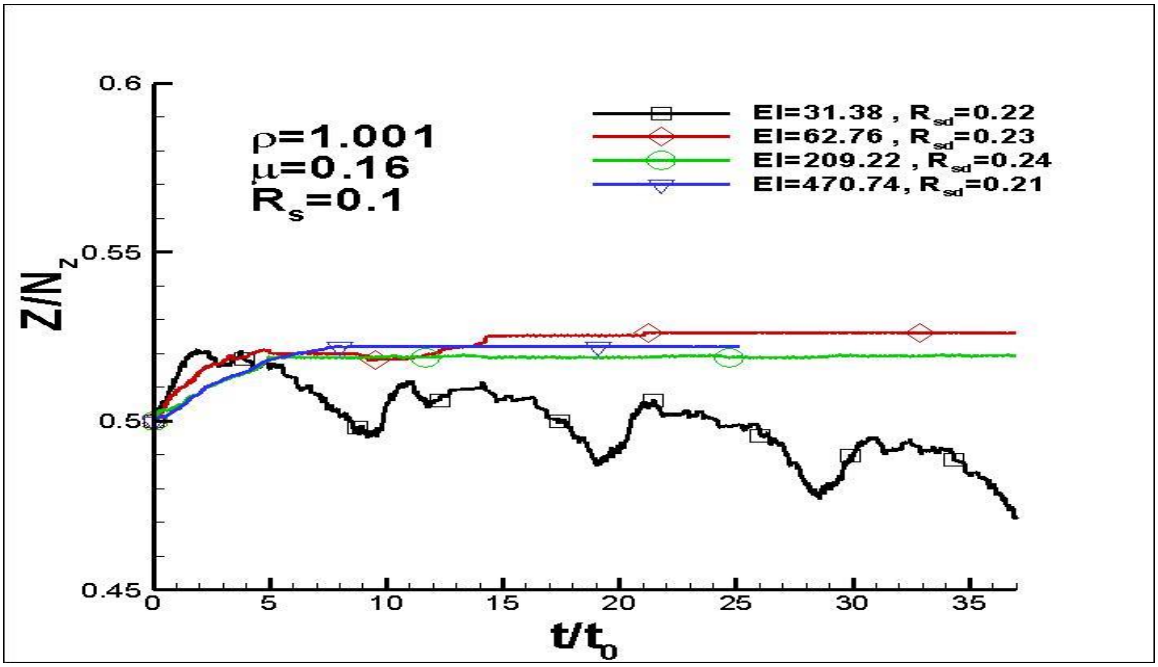

Figure 16: Magnification of Figure 15

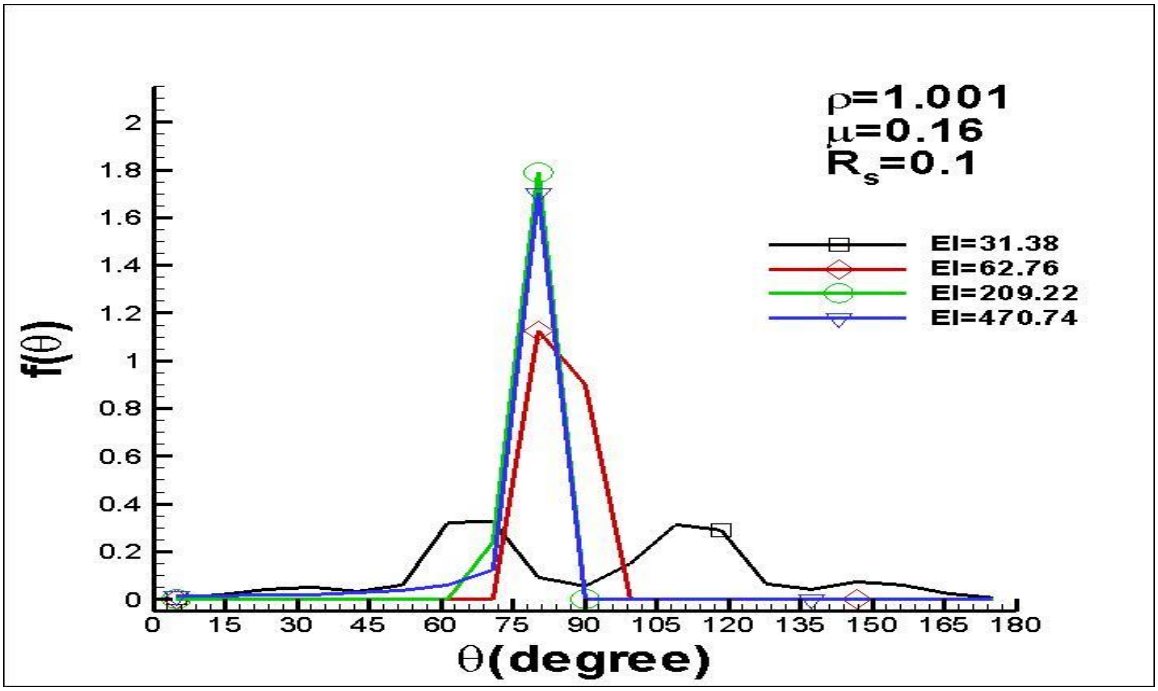

Figure 17: The Angle Probability of the Fiber During the Migration

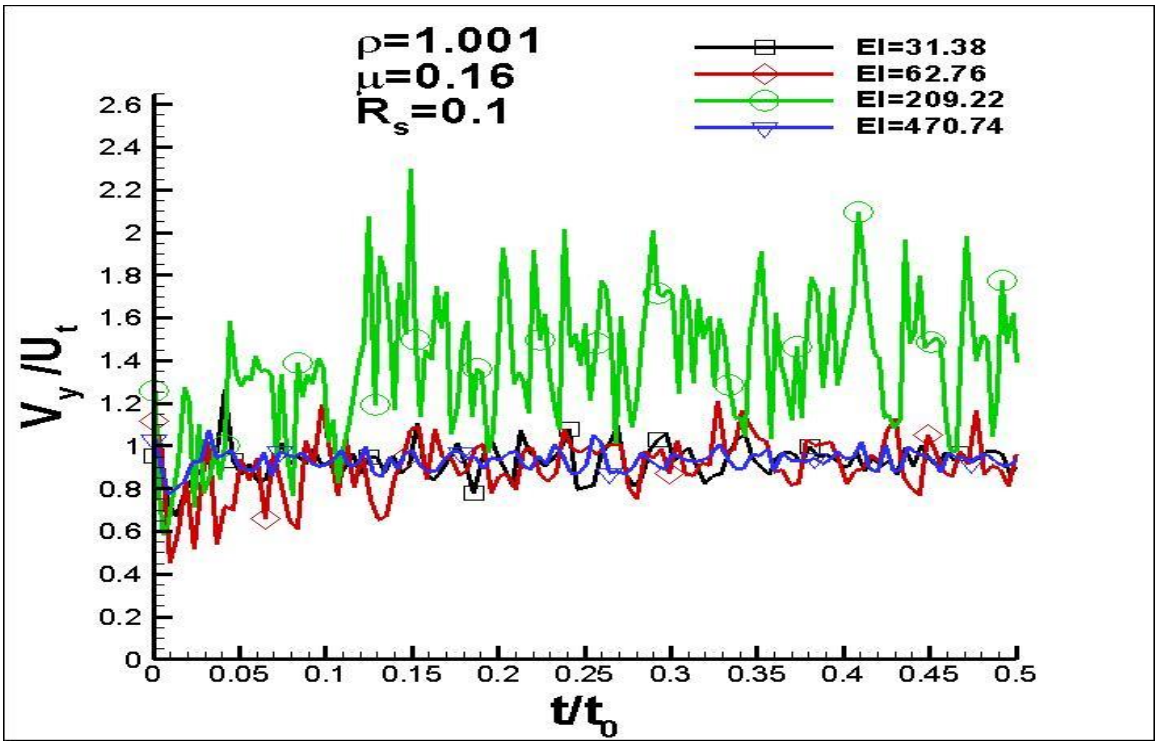

Figure 18: The Fiber's Velocities in the Gravity Direction of a Weak Vertical Shear Flow

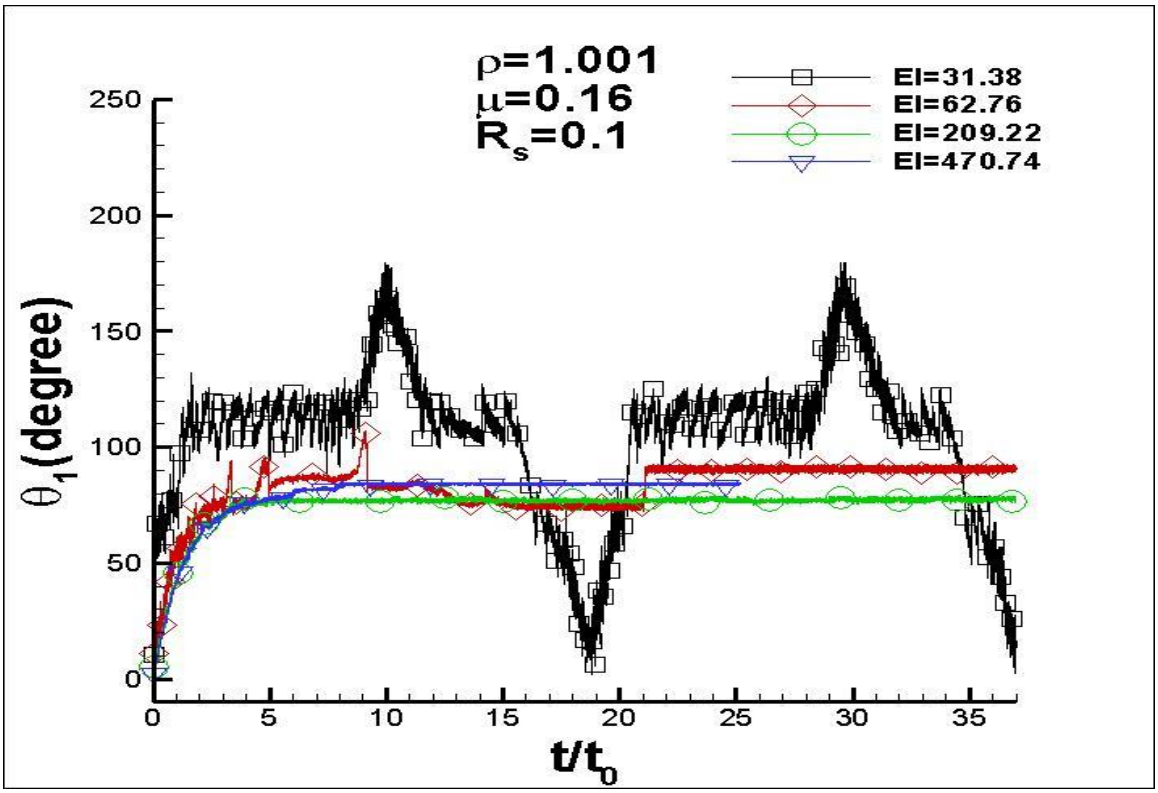

Figure 19: The Angle of the Ninth Segment of the Fiber in a Weak Vertical Shear Flow

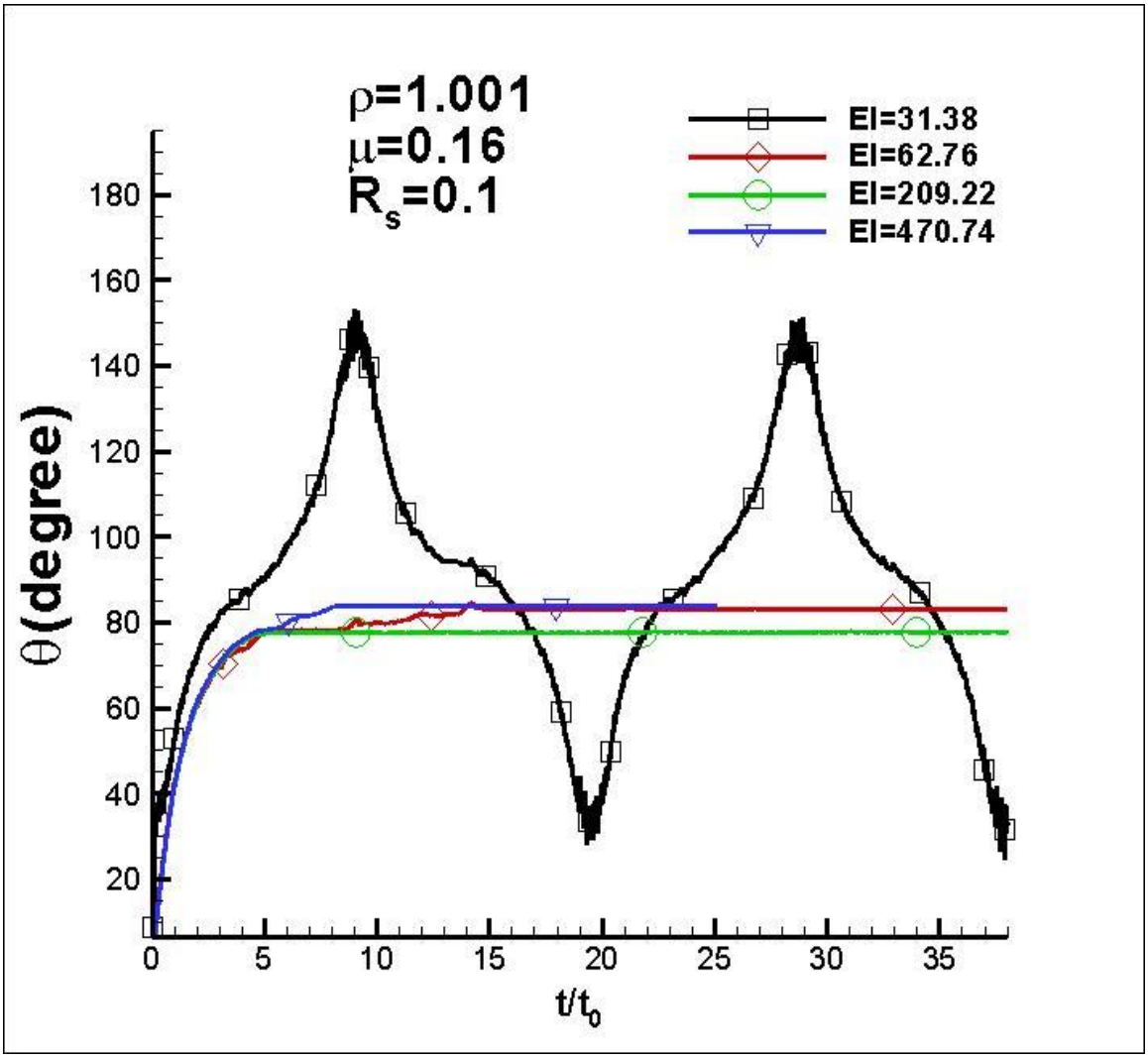

Figure 20: The Angle Average of the Fiber in a Weak Vertical Shear Flow

5.4 Effects of Vertical Shear Flow

To study the influence of the vertical shear, additional two levels of shear Reynolds numbers R_S=0.2 and R_S=0.3 are used in the simulations. The fiber density is kept at 1.001 and the four different rigidities (EI=31.38, EI=62.76, EI=209.22, and EI=470.74) are utilized.

When R_S increases from 0.1 to 0.2, the final position of the most flexible fiber with EI= 31.38 moves from Z=0.33 to Z=0.29, more close to the wall of Z=0.0. as shown in figures 15 and 21, because a larger shear force may push fiber move to the wall of Z=0 more closely and cause fiber to be dispersed more, signifying that the dispersion tendency increases as the shear Reynolds number increases for the most flexible fiber case. When the shear rate increases, the fiber inertia effects become relatively weaker. Therefore the fibers migrate to the area more close to the wall of Z=0 due to the stronger shear flow. In these cases, the inertia of a fiber plays less important role because it is dominated by the shear flow.

The final positions of other stiffer fibers with EI=62.76, 209.22, and 470.74 are around Z=0.52 N_Z when R_S=0.1 while the final positions of the corresponding fibers are around 0.51 N_Z when R_S=0.1. The two figure comparison suggests that a larger shear force also reduces the coagulation ability of these fibers.

It is interesting that when shear Reynolds number continuously increase to 0.3, not only the most flexible fiber of EI= 31.38 but also the next flexible fiber with EI=62.76 moves to the dispersion area with final position less than Z=0.5 N_Z although the final

position of the next flexible fiber with EI=62.76 is larger than Z=0.5Nz for both R_S =0.1 and 0.2, evidencing that a large shear force may convert fiber from a coagulation state to dispersion state. Under the shear force, the final positions of the other stiffer fibers of EI=209.22 and EI=470.74 are reduced as compared in figure21 and 27; the tendency of the coagulation is reduced.

Figure 21 and Figure 27 show the position of each fiber during the migration. Figure 23 and Figure 29 show the angle probability of each fiber. Figure 24 and Figure 30 show the fibers' velocities in the gravity direction. Figure 25 and Figure 31 show the angle of the ninth segment of a fiber, and the most rigid fibers do not have wide angles. Unlike, the most flexible fibers are the most deformable fibers, and that makes the fibers have wide angles during the migration. Figure 26 and Figure 32 show the angle average of all fiber's segments.

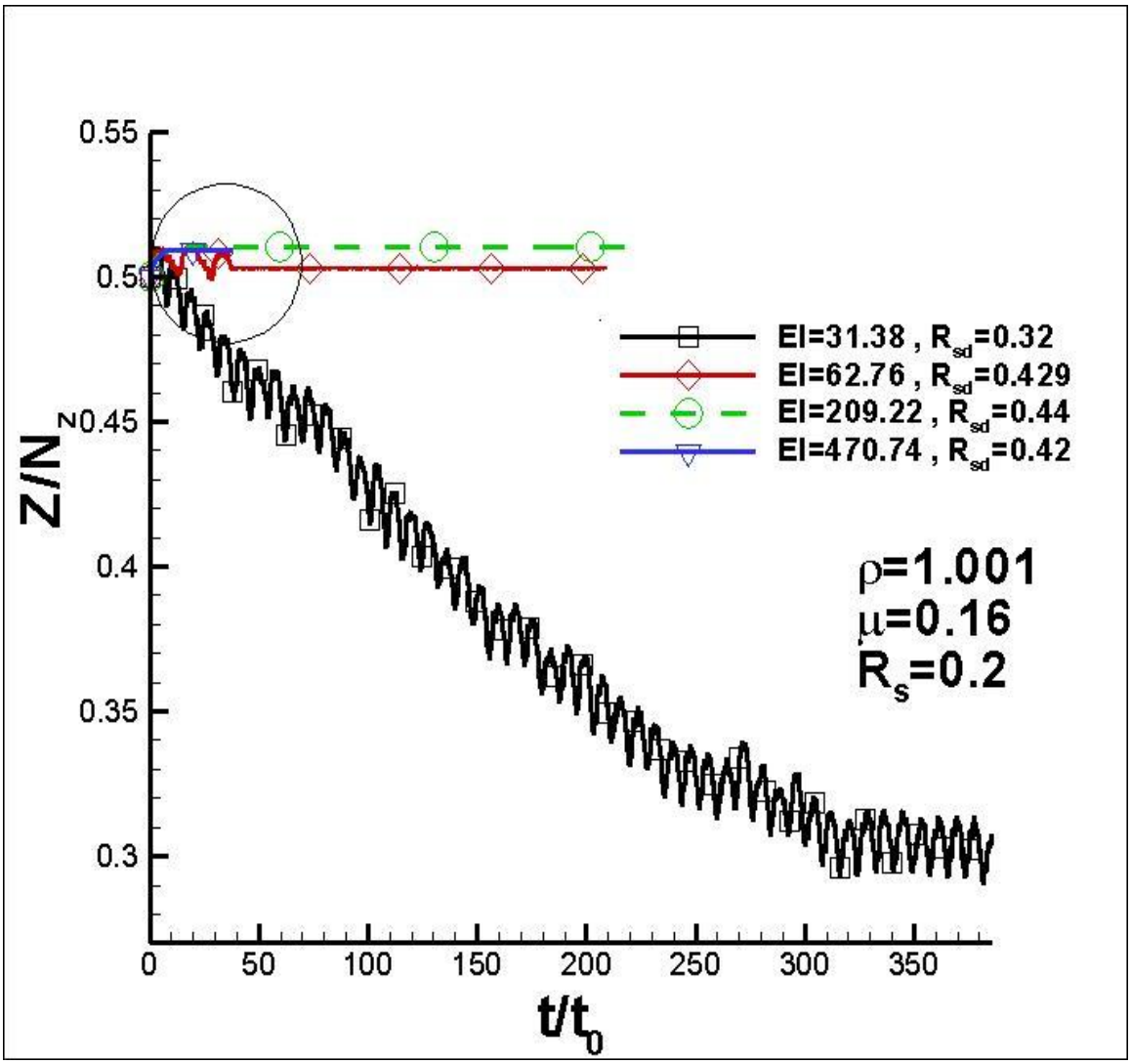

Figure 21: The Fiber Lateral Migration in a Vertical Weak Shear Flow

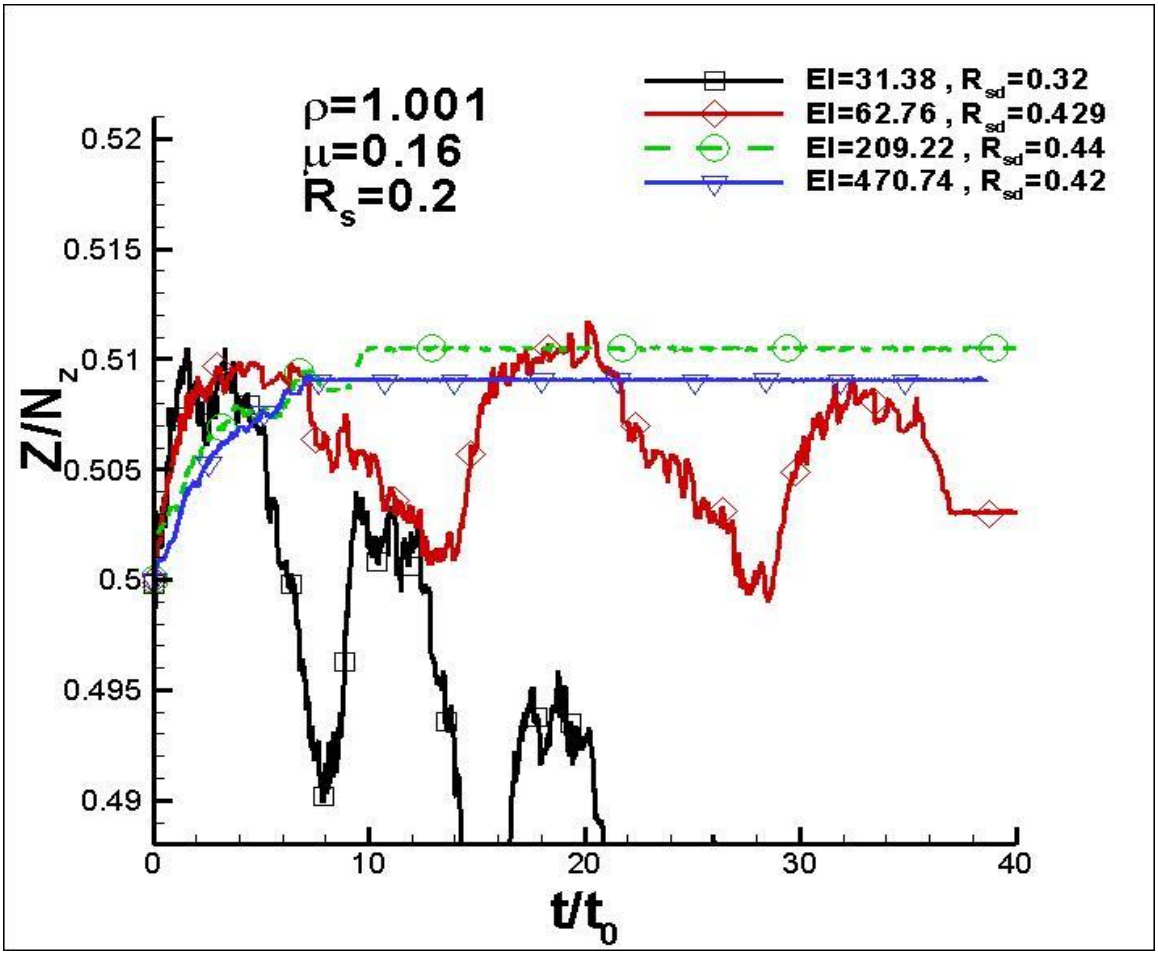

Figure 22: Magnification of Figure 21

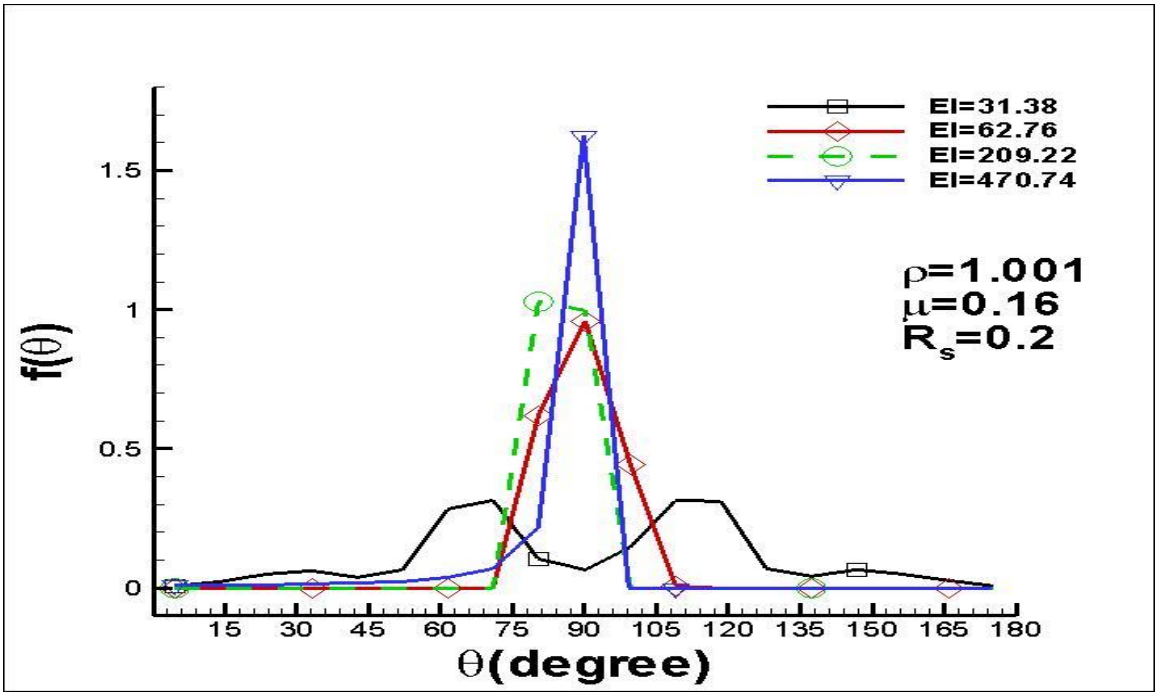

Figure 23: The Angle Probability of the Fiber During the Migration

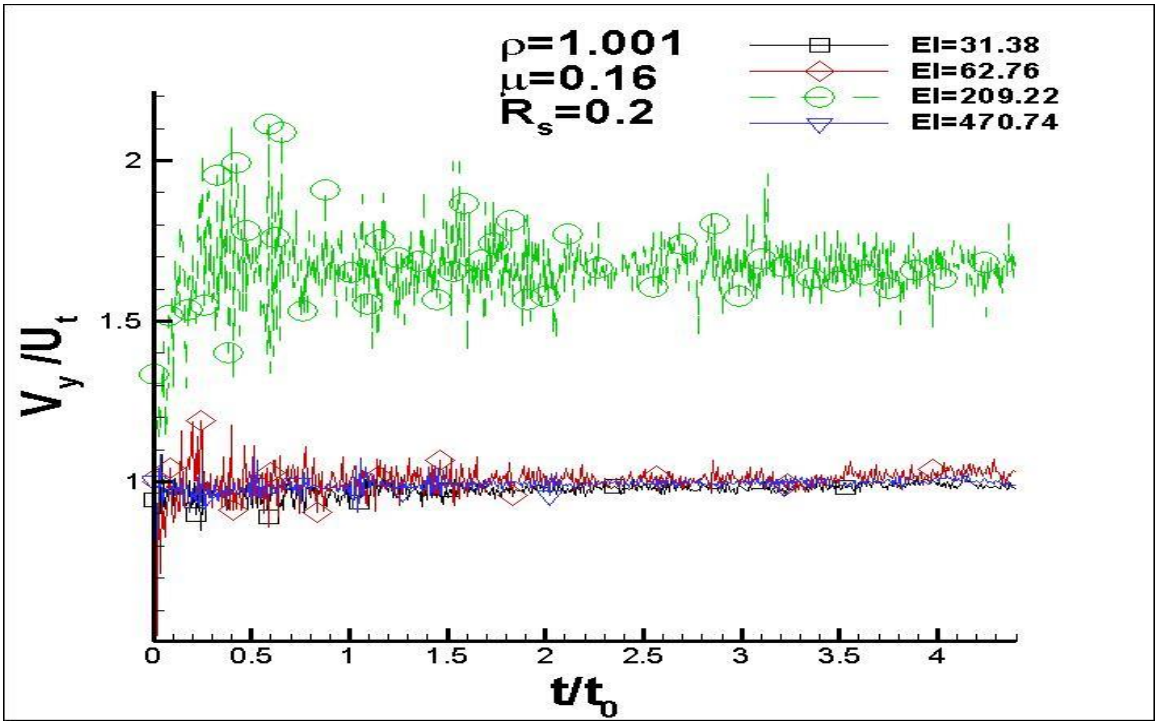

Figure 24: The Fiber's Velocities in the Gravity Direction of a Weak Vertical Shear Flow

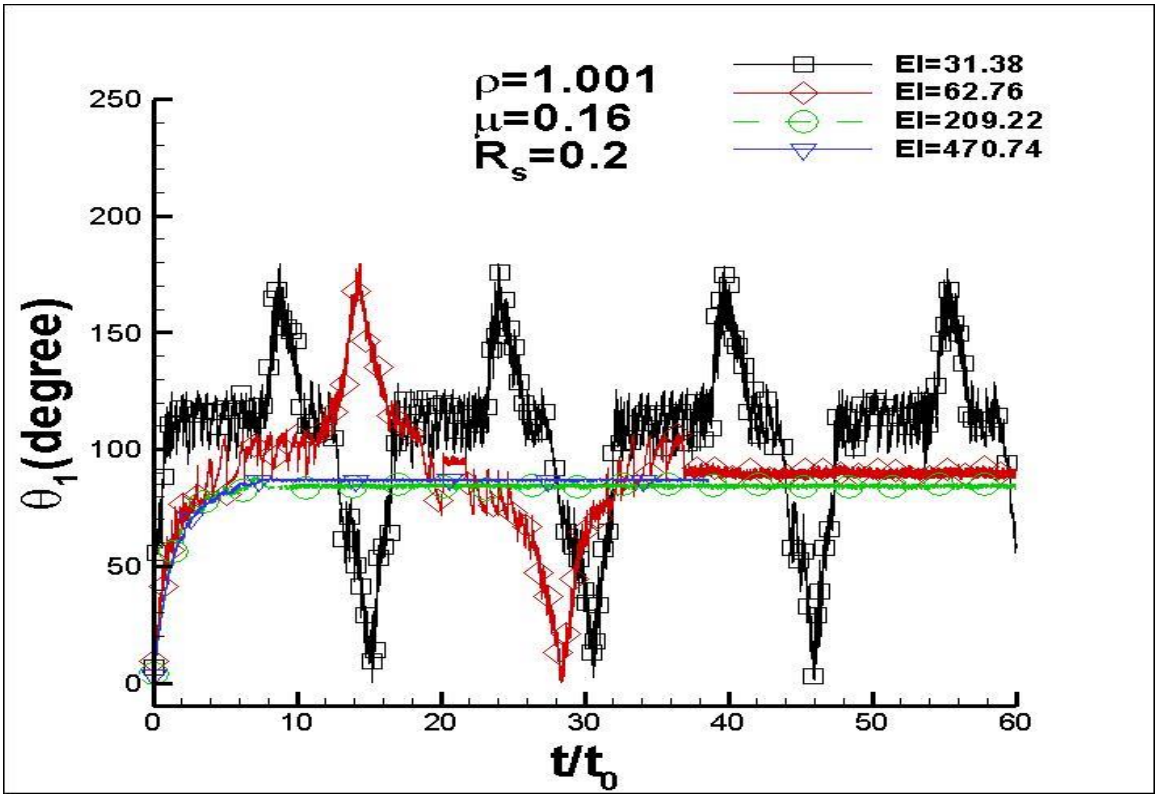

Figure 25: The Angle of the Ninth Segment of the Fiber in a Weak Vertical Shear Flow

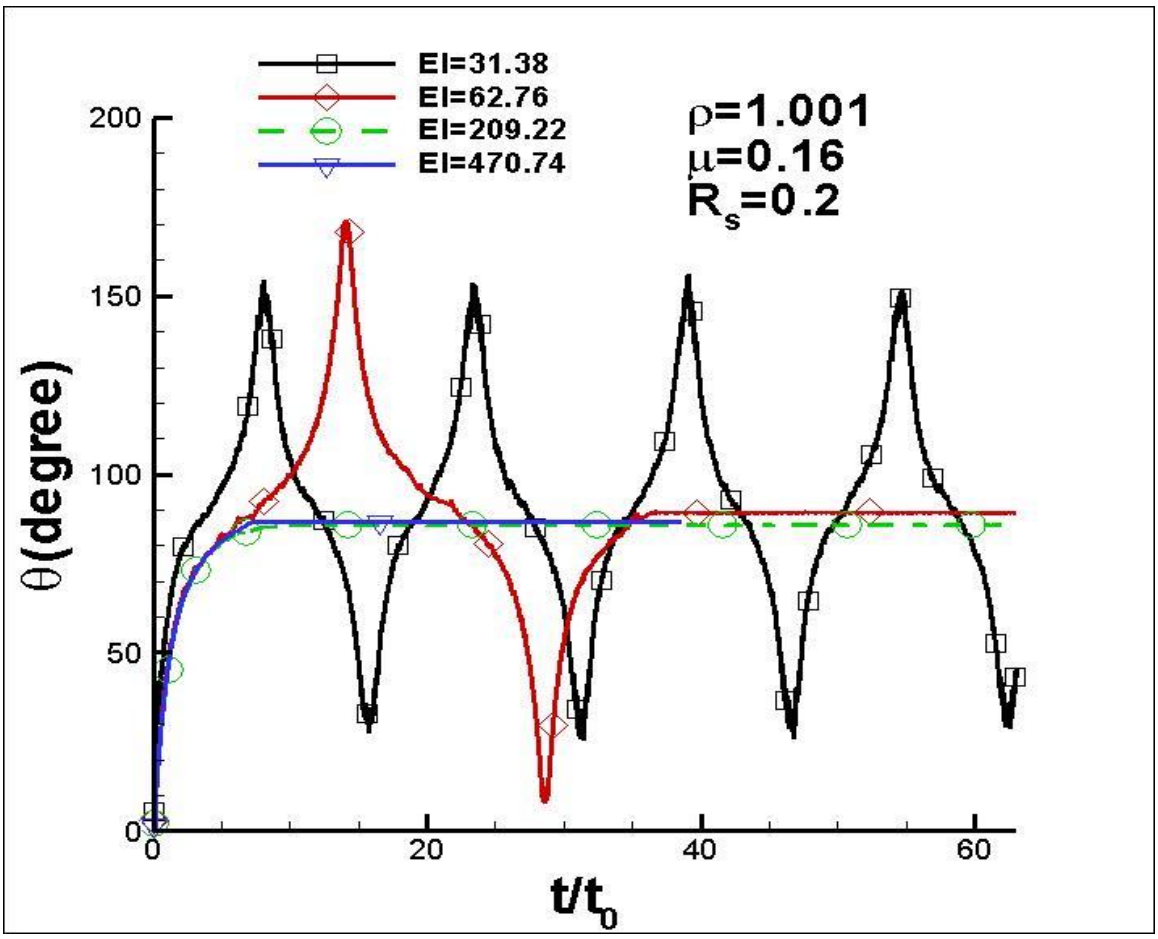

Figure 26: The Angle Average of the Fiber in a Weak Vertical Shear Flow

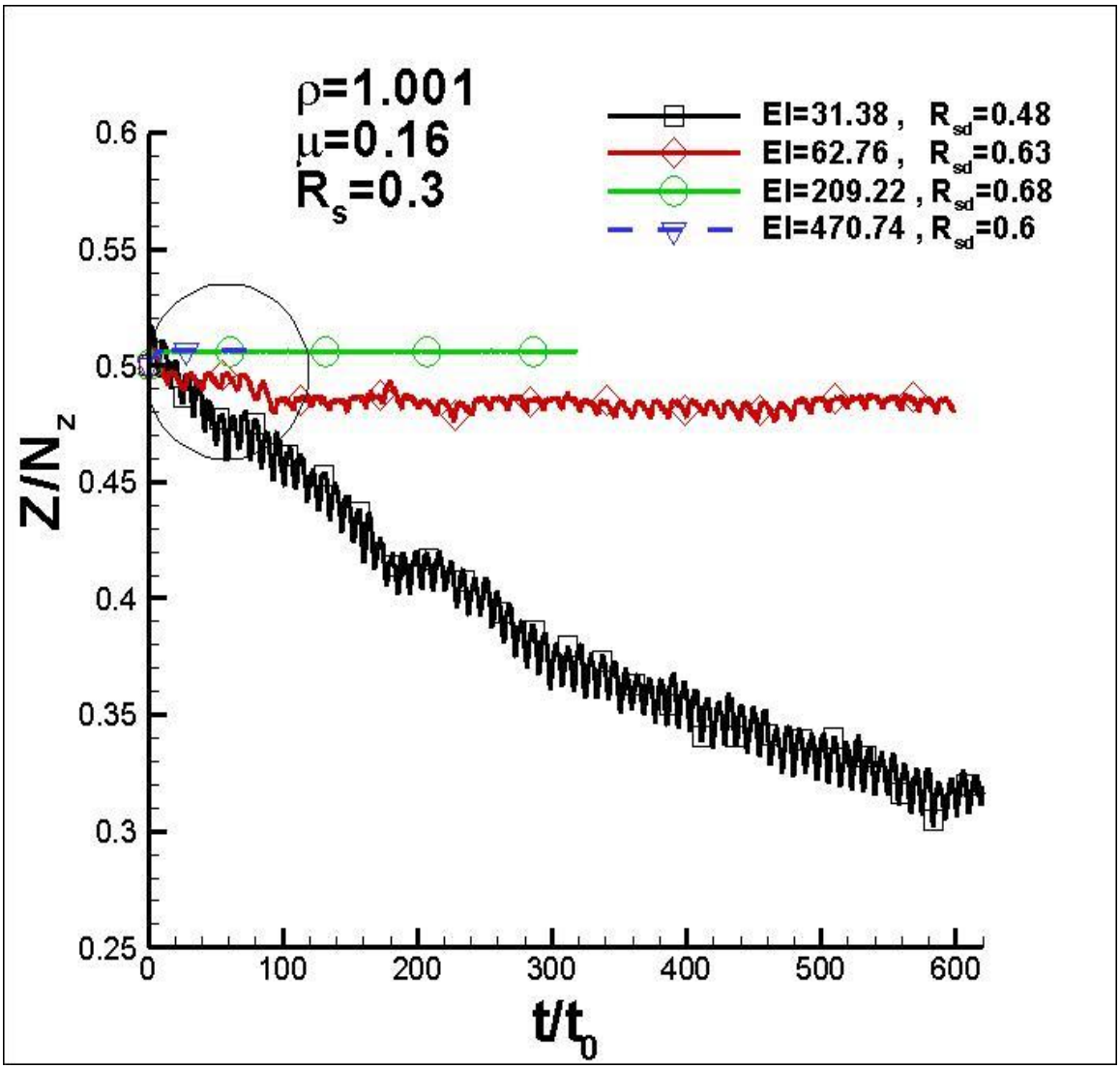

Figure 27: The Fiber Lateral Migration in a Vertical Shear Flow

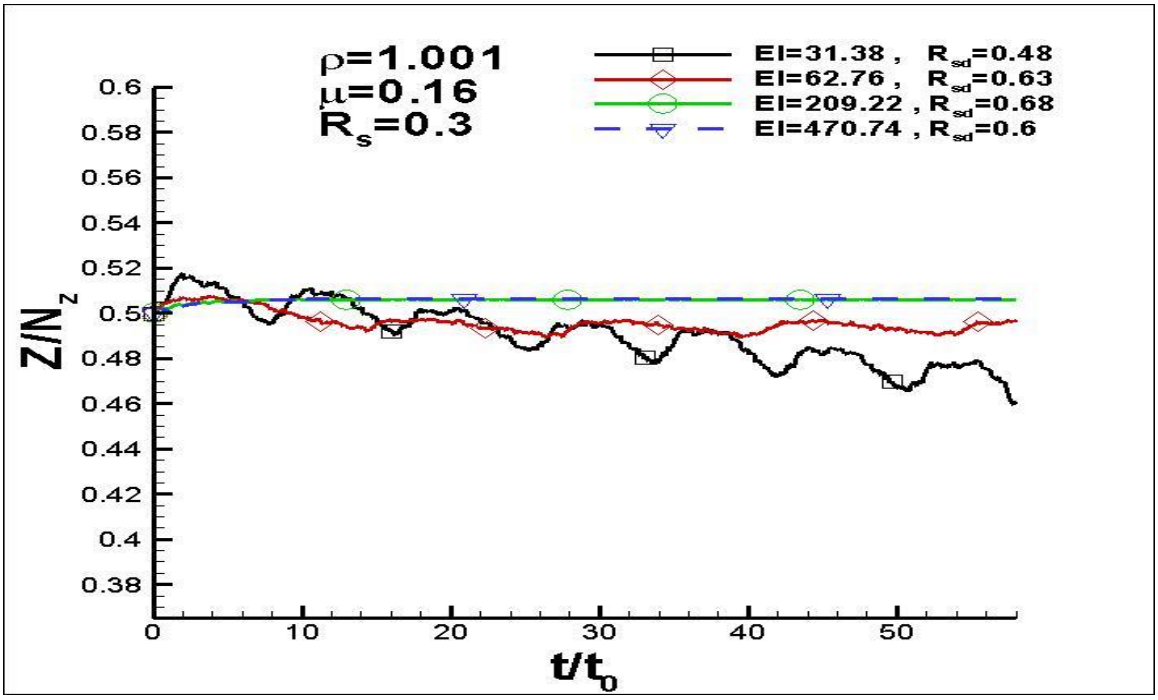

Figure 28: Magnification of Figure 27

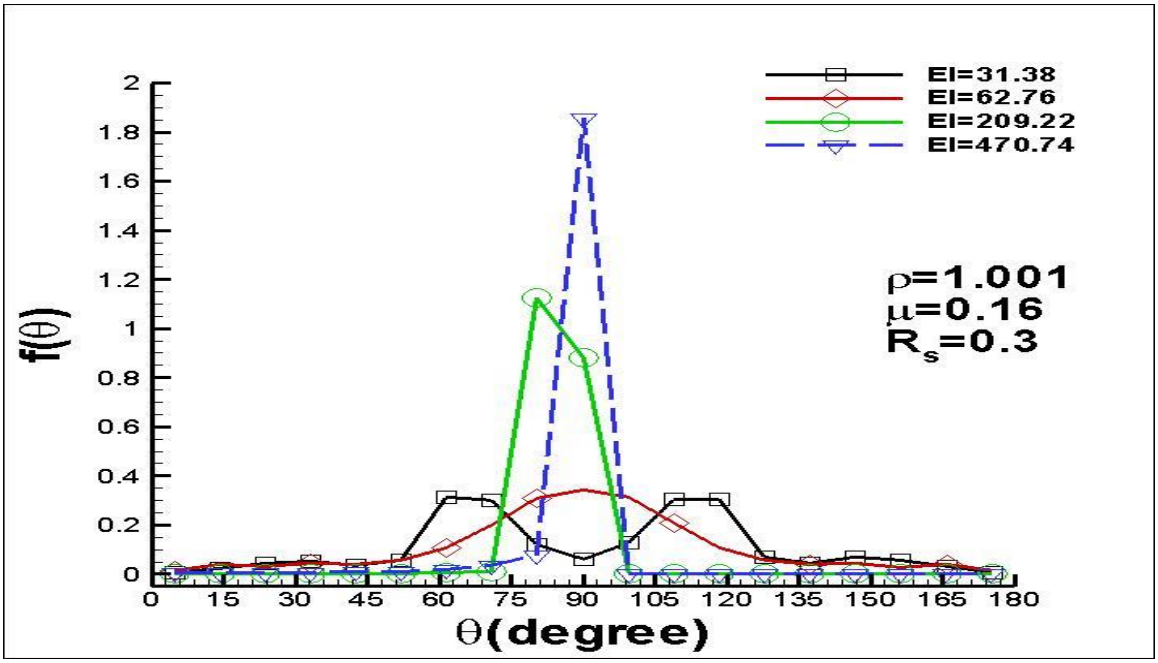

Figure 29: The Angle Probability of the Fiber During the Migration

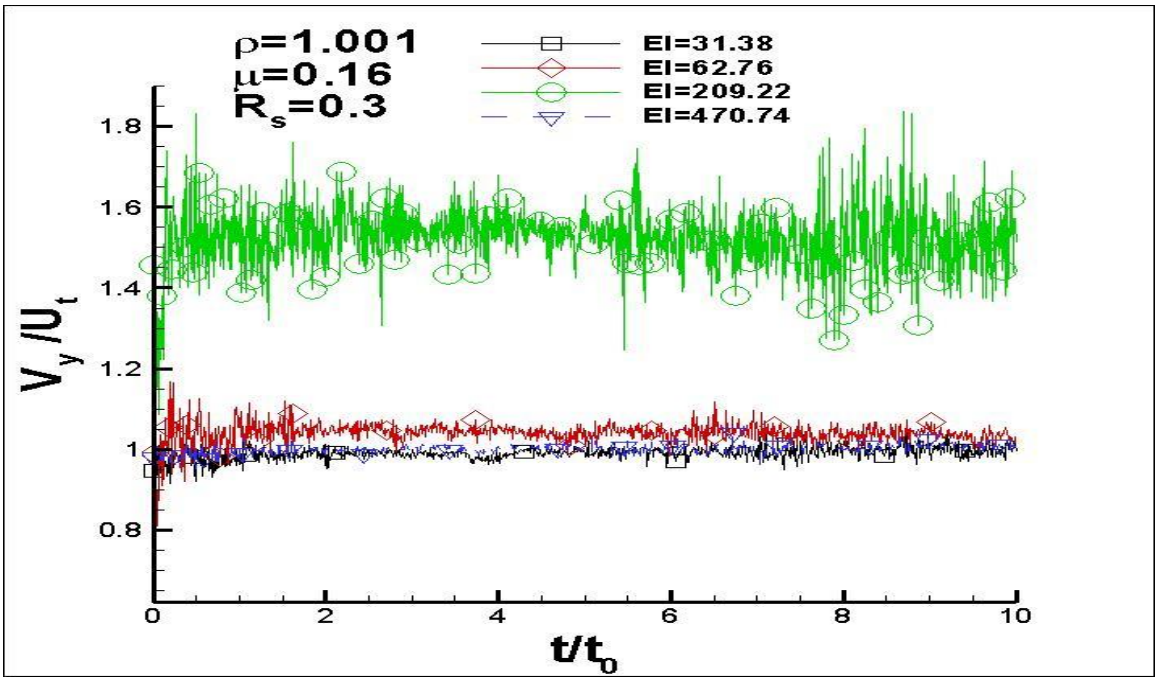

Figure 30: The Fiber's Velocities in the Gravity Direction of a Weak Vertical Shear Flow

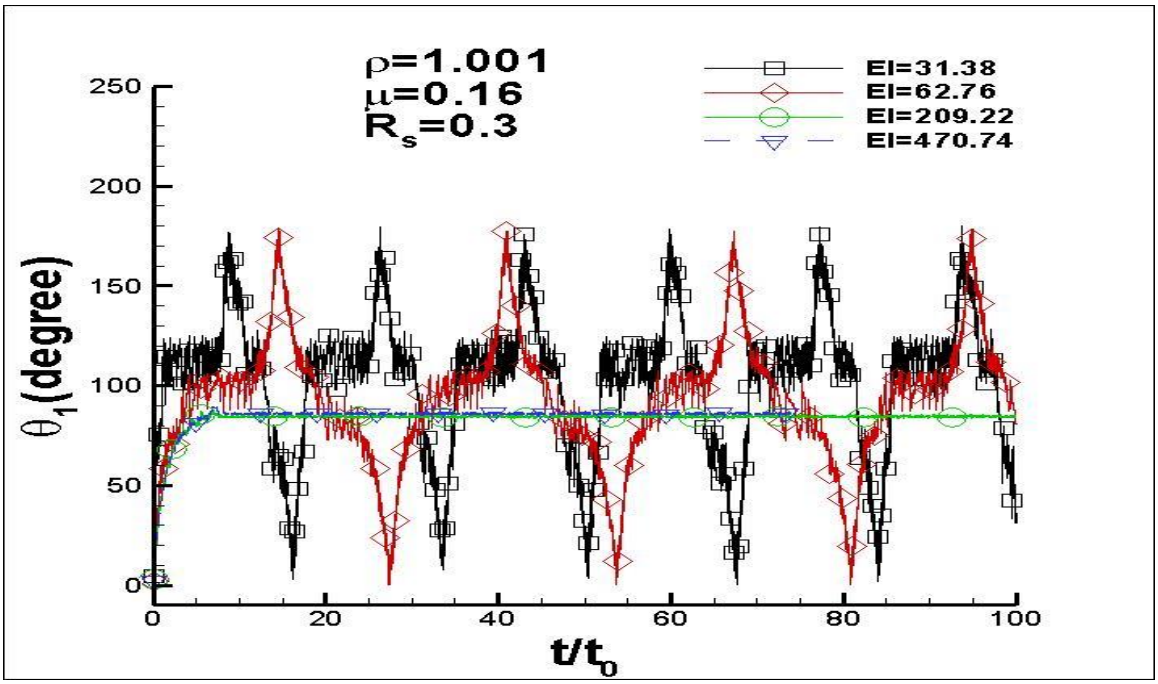

Figure 31: The Angle of the Ninth Segment of the Fiber in a Weak Vertical Shear Flow

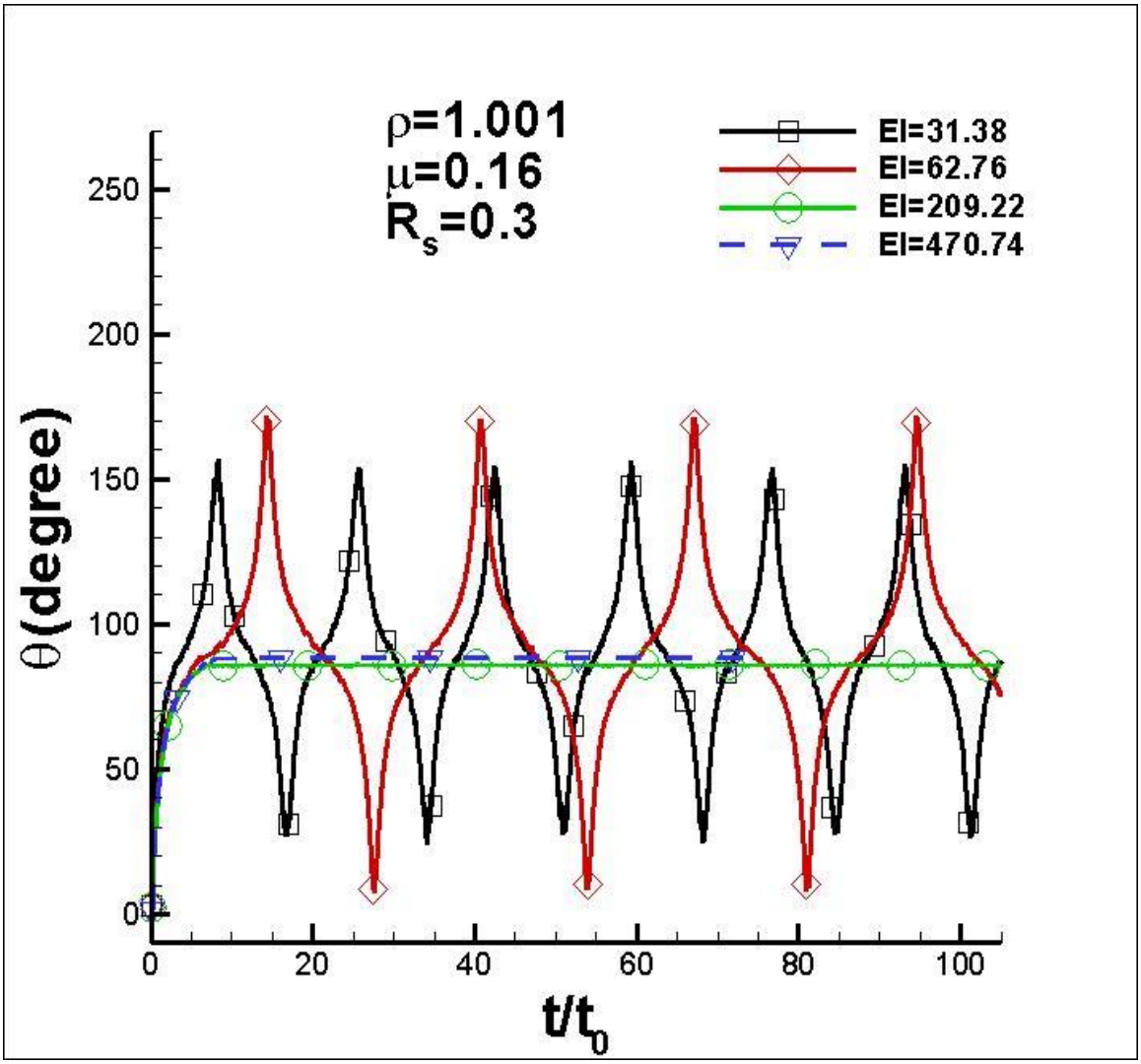

Figure 32: The Angle Average of the Fiber in a Weak Vertical Shear Flow

CHAPTER VI

DISCUSSION AND CONCLUSION

Particulate flows have extensive applications in chemical engineering, science and industries. For example, sedimentation, filtration, and screening are normally used to separate solid particles from fluids in pharmaceutical, petroleum, food process as well as paper industry; sands will settle down in ocean and rivers which has an effect on environments; the blood-based particles (plaque) may deposit on the artery and cause heart disease; these examples illustrate the importance of particle suspension flows. This is the reason why engineers and scientists have paid a great attention to this subject in both experimental and theoretical studies.

This work focuses on motion of settling flexible particle in a vertical weak shear flow and the influence of rigidity of a fiber on lateral migration is studied. This subject is directly related to the stability of fiber suspension.

Sedimentation is the process of particles settling by gravity in a fluid. When fibers are settling, a weak vertical shear flow may be established within the suspension. In other words, the weak vertical shear flow is generated from the variation of the fiber number density in the fluid. A fiber within the suspension may experience the shear force and laterally migrate either toward the downward flowing fluid region with the high particle number density, which is called coagulation or toward the lower particle number density region which is called dispersion, depending on the settling Reynolds numbers, defined by $R_{sd} = V_f . l / 2\upsilon$, where V_f is the terminal settling velocity of the mass center of the

fiber in the gravity direction or y-direction; l is the fiber length; and ν is the kinematic viscosity.

Several simulations are conducted. In the simulation, a vertical weak shear flow is constructed. The velocity of the left wall of the simulation box at Z=0 is set equal to zero. The right wall at Z=L has a velocity of V_0 in vertical direction, where L is the channel width. The shear rate $G = V_0/L$. The shear Reynolds number R_s is defined by $R_S = G\ l^2 / 4\nu$ where l is the fiber length; ν is the kinematic viscosity.

6.1 Effects of Rigidity on Lateral Migration When $R_{sd} > 1.0$

In the case, the fiber density is 1.1 and the shear Reynolds number 0.1 is given. The rigidity is varied at different levels of EI=31.38, EI=62.76, EI=209.22, and EI=470.74.

The simulation results show that the fiber settles down vertically by gravity and the fiber oscillates in the Z-direction first, then becomes stable and final is stopped at the area of $Z/N_Z > 0.5$, indicating that the fiber tends to migrate to the coagulation region or the higher fiber density area when the settling Reynolds number is larger than 1.0. This is consistent with previous theoretical prediction of Kang (2009) and simulation results of Guo (2013) for the rigid fiber [2][3]. The inertia of the fiber turns its long axis along the horizontal direction while the vertical shear flow tries to resist this inertial rotation. As a result, there is a small inclined angle between the fiber long axis and the horizontal direction. With this inclined angle, the fiber laterally migrates to the fiber high density area until the wall repulsive force stops the migration.

It is clearly observed that at this Reynolds number range, a fiber with an intermediate rigidity migrates to a position where is the most close to the wall in the coagulation area and the fiber receives the largest wall repel force. It concludes that when R_{sd} is large, as rigidity increases the lateral migration with $V_Z > 0$ increases, as the rigidity continues to increases to an optimized level, the lateral migration becomes the largest, indicating that the fiber with an intermediate rigidity has the largest tendency to migrate to the coagulation area. This is because an intermediately rigid fiber has a larger inertia which turn fiber long axis along the inclined angle and results in a larger migration with $V_Z > 0$.

6.2 Effects of Rigidity on Lateral Migration When $R_{sd} < 1.0$

As settling Reynolds number decrease to a level of $R_S < R_{sd} < 1.0$, the shear flow plays more function. At this small settling Reynolds number, the shear flow may push fiber to the position of $Z/N_Z < 0.5$, the area of dispersion.

At the low settling Reynolds number $R_{sd} < 1$, as rigidity decrease, the fiber may migrate to a position more close to the position close to Z=0; as the rigidity increases, the fiber may move to the position of $Z/N_Z > 0.5$. In other words, the rigidity can convert fiber from a dispersion area to a coagulation area.

It is concluded that the stability of a fiber suspension is dependant of rigidity.

BIBLIOGRAPHY

[1] Qi, D. (2006). Direct Simulations of flexible cylindrical fiber suspensions in finite Reynolds number flows. The Journal of Chemical Physics: Western Michigan University.

[2] Qi, D., & Gordnier, R. (n.d.) (2014). Effects of deformation on lift and power efficiency in a hovering motion of a chord-wise flexible wing. Journal of Fluids and Structures: Western Michigan University.

[3] Qi, D., He, Guo,& Liu, Y. (2013). Lattice Boltzmann simulations of sedimentation of a single fiber in a weak vertical shear flow. AIP Physics of Fluids: AIP Publishing LLC.

[4] Wu, T., Guo, R., He, G., Liu, Y., & Qi, D. (2014). Simulation of swimming of a flexible filament using the generalized lattice-spring lattice-Boltzmann method. Journal of Theoretical Biology: Elsevier Ltd.

[5] Chiang, Shio-Hung. (). Solid-Liquid Separation. University of Pittsburgh.

[6] Bird, R., and W. Stewart. (1960). Transport phenomena, Second ed. New York: University of Wisconsin. (p. 895).

[7] Coulson. J.M., and J.F. Richardson, J.R. Backhurst, J.H. Harker. (1999). Chapter 2: Flow of Fluids- Energy and Momentum Relationships. In Coulson and Richardson's Chemical Engineering: Fluid Flow, Heat Transfer, and MassTransfer, Vo. 1, 6th Ed. Oxford: Butterworth-Heinmann.

[8] Coulson. J.M., and J.F. Richardson, J.R. Backhurst, J.H. Harker. (1999). Chapter 7: Liquid Mixing. In Coulson and Richardson's Chemical Engineering: Fluid Flow, Heat Transfer, and MassTransfer, Vo. 1, 6th Ed. Oxford: Butterworth-Heinmann.

[9] Richardson, J.F. and J.H. Harker and J.R. Backhurst. (2002). Chapter 3: Mothion of Particles in a Fluid. In Coulson and Richardson's Chemical Engineering: Particle Technology and Separation Processes, Vol. 2, 5th Ed. Oxford: Butterworth Heinemann.

[10] Richardson, J.F. and J.H. Harker and J.R. Backhurst. (2002). Chapter 5: Sedimentation. In Coulson and Richardson's Chemical Engineering: Particle Technology and Separation Processes, Vol. 2, 5th Ed. Oxford: Butterworth Heinemann.

[11] Richardson, J.F. and J.H. Harker and J.R. Backhurst. (2002). Chapter 6: Distillation. In Coulson and Richardson's Chemical Engineering: Particle Technology and Separation Processes, Vol. 2, 5th Ed. Oxford: Butterworth Heinemann.

[12] Wu,,Tai-Haien and Qi, Dewi (2014) "Advantage of a finite Extensible Nonlinear Elastic Potential in Lattice Boltzmann Simulation," The Hilltop Review: Vol.7:lss.1, Article 10.

[13] Shuling ,H. (1995). “Chapter 3: The Two –Dimensional Square Lattice Boltzman Model”. Lattice Boltzman Method for Incompressible Viscous Flow. UMI Company: Ann arbour, Michigan, USA.

[14] Sinnott, R.K. (2005). Chapter 2: Fundamentals of Material Balances. In Coulson and Richardson’s Chemical Engineering: Particle Technology and Separation Processes: Chemical Engineering Design, Vol. 6, 4th Ed. Oxford: Butterworth Heinemann.

[15] Sinnott, R.K. (2005). Chapter 3: Fundamentals of Energy Balances (and Energy Utilisation). In Coulson and Richardson’s Chemical Engineering: Particle Technology and Separation Processes: Chemical Engineering Design, Vol. 6, 4th Ed. Oxford: Butterworth Heinemann.

[16] Sinnott, R.K. (2005). Chapter 11: Separation Columns (Distillation, Absorption, and Extraction). In Coulson and Richardson’s Chemical Engineering: Particle Technology and Separation Processes: Chemical Engineering Design, Vol. 6, 4th Ed. Oxford: Butterworth Heinemann.

[17] Sinnott, R.K. (2005). Chapter 12: Heat-transfer Equipment. In Coulson and Richardson’s Chemical Engineering: Particle Technology and Separation Processes: Chemical Engineering Design, Vol. 6, 4th Ed. Oxford: Butterworth Heinemann.

[18] Sinnott, R.K. (2005). Chapter 13: Mechanical Design of Process Equipment. In Coulson and Richardson’s Chemical Engineering: Particle Technology and Separation Processes: Chemical Engineering Design, Vol. 6, 4th Ed. Oxford: Butterworth Heinemann.

[19] Smith, J.M. and H.C. Van Ness and M.M. Abbot. (2005). Appendix C. In Introduction to Chemical Engineering Thermodynamics (in SI Units), 7th Ed. New York: McGraw Hill.

APPENDIX

1. $\vec{U}_b$ -- boundary velocity of the solid segment
2. τ -- single relaxation time
3. θ_L -- leading edge angle
4. $\vec{\Omega}$ -- angular velocity of the solid segment
5. $\vec{c}_i^{+}$ -- semi-axis vector of the wing segment in the body-fixed coordinate system
6. $\vec{F}_i^h$ -- total hydrodynamic force on solid particle i
7. $\vec{F}_i$ -- total force on segment i$\vec{}$
8. $\vec{R}_i$ -- position vector of the mass center of solid segment i
9. $\vec{T}_i^h$ -- total hydrodynamic torque on solid particle i
10. a_3 -- length of the semi-axis of the wing segment along the chord
11. $f_\sigma(\vec{x},t)$ -- fluid particle distribution function
12. $f_\sigma^{eq}(\vec{x},t)$ -- equilibrium distribution function
13. I -- inertial moment
14. $\alpha 0$ -- initial pitch angle
15. $\alpha 1$ -- amplitude of pitch motion
16. a_2 -- phase angle
17. $\Delta\theta_B$ -- trailing edge deflection angle
18. $\Delta\theta_L$ -- leading edge deflection angle
19. δt -- length of time step

20. ε -- Knudsen number

21. κ -- reduced frequency

22. ν -- kinematic viscosity

23. ω -- flapping angular velocity

24. ω^* -- Normalized frequency

25. ω_0 -- Nature frequency

26. ω_σ -- weight coefficient

27. $\prod_0$ -- effective inertia

28. ρ_f -- fluid density

29. ρ_s -- wing density

30. σ -- direction number of the particle discrete velocity

31. θ -- pitch angle

32. Θ_i -- bending angle between the ith and (i+1)th segment

33. θ_T -- trailing edge angle

34. $\vec{e}_\sigma$ -- particles discrete velocity

35. $\vec{C}_i^+$ --vector from the mass center of the segment i to the joint

36. $\vec{F}$ -- hydrodynamic force

37. $\vec{G}_i$ -- constraint force on joint i

38. $\vec{G}_{ti}$ -- total constraint force on the ith segment

39. $\vec{T}_{ti}^b$ -- total bending torque

40. $\vec{T}_{ti}^{G}$ -- total torque due to the constraint force

41. $\vec{u}$ -- Fluid velocity

42. $\vec{x}$ -- position vector of the fluid boundary node

43. $\vec{x}_b$ -- position vector of the solid boundary node

44. c -- chord length

45. C_d -- drag coefficient

46. C_l Cl -- lift coefficient

47. E -- Young's modulus

48. EI_l -- bending flexural rigidity

49. f -- flapping frequency

50. F_f -- non-dimensional hydrodynamic force per unit chord length

51. f_P -- power efficiency

52. F_z -- total hydrodynamic force in the z-direction

53. H -- amplitude of the plunge

54. h -- wing thickness

55. I_l -- second moment of area

56. l -- coordinate variable along the chord direction

57. M -- mass of segment

58. $O_z^{'}$ -- pitch angular velocity

59. P -- power input coefficient

60. p -- pressure

61. Re -- Reynolds number

62. s -- span length

63. t_+ -- time after fluid particle collision

64. t_0 -- short time scale

65. t_1 -- long time scale

66. U_0 -- reference velocity

67. U_0 -- angular velocity amplitude

68. w -- bending displacement

69. A_i -- rotational transformation matrix of segment i

70. N -- number of the segment

71. $\vec{U}_c$ -- velocity of the mass center of solid segment